PALACKY UNIVERSITY OLOMOUC
FACULTY OF NATURAL SCIENCES

Department of Optics

Characterization of polarization-maintaining fibers

Bachelor Thesis

Robert Stárek

2013

PALACKY UNIVERSITY OLOMOUC
FACULTY OF NATURAL SCIENCES

Department of Optics

Characterization of polarization-maintaining fibers

BACHELOR THESIS

Author:	Robert Stárek
Study programme:	B1701 Physics
Field of study:	Optics and optoelectronics
Form of study:	Full - time
Supervisor:	Mgr. Michal Mičuda, Ph.D.
Co-supervisor:	Mgr. Miroslav Ježek, Ph.D.

UNIVERZITA PALACKÉHO V OLOMOUCI
PŘÍRODOVĚDECKÁ FAKULTA

Katedra Optiky

Charakterizace vláken udržujících polarizaci

BAKALÁŘSKÁ PRÁCE

Autor:	Robert Stárek
Studijní program:	B1701 Fyzika
Studijní obor:	Optika a optoelektronika
Forma studia	Prezenční
Vedoucí práce:	Mgr. Michal Mičuda, Ph.D.
Konzultant:	Mgr. Miroslav Ježek, Ph.D.

Abstract

Optical fibers are important tools for modern communications. Properties of signal, such as duration of pulse or polarization state are changed by propagation in fiber. These changes can increase error occurrence in transmitted information. The goal of this experimental-oriented thesis is characterization of polarization-maintaining fibers and technical aspects of their use.

Keywords

Declaration

I declare that I have written Bachelor Thesis "Characterization of polarization-maintaining fibers" on my own under the guidance of Mgr. Michal Mičuda, Ph.D. by using theoretical resources, which are referred to in the list of literature. I agree with the further usage of this document according to the requirements of the Department of Optics.

Declared in Olomouc on ....

Signature ....

Contents

1 Introduction

Optical fibers are widely used for modern communications. Information can be encoded into various properties of light. One of them is polarization. However, non-polarization-maintaining fibers are not suitable for transmission of polarization-encoded information - mechanical stress and thermal fluctuation within the fiber cause birefringence and cross talk between polarization modes. Therefore output polarization is not under our control.

The answer to this problem are polarization-maintaining fibers. They are based on intentionally stress-induced birefringence within the fiber. Intentional stress is greater than stress caused by outer factors, therefore outer factors could be neglected and polarization-maintaining fiber should maintain linear polarization along its two axes - the slow and the fast.

There are several ways of inducing stress in fiber. Figure 1 shows "panda" and "bow-tie" styles of stress members.
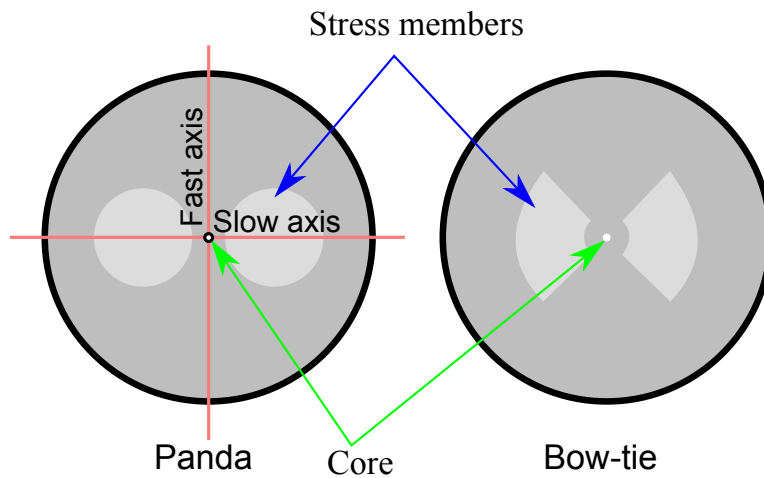
Figure 1: Stress members could be implemented several ways. Cross section shows "panda" and "bow-tie" style of stress-members in polarization-maintaining fiber.

We were working exclusively with "panda" style fibers. Due to nature of polarization we need to keep angular position of the fiber under control. Fiber connector has a "key" (see photo in Figure 2) that fits into a "keyhole" of device (such as collimator decoupler in Figure 3) preventing change of angular position. Some optical fibers have removable key but polarization maintaining fibers have fixed key.
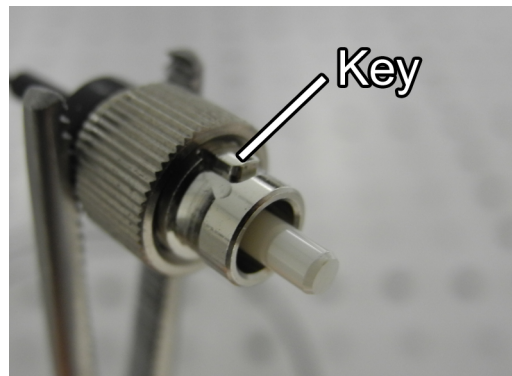
Figure 2: Photo of polarization-maintaining fiber FC/PC connector.

Figure 3: Photo of polarization-maintaining fiber connected to collimator. Connector key fits into keyhole so we have angular position of the fiber under control.

If we could somehow maintain arbitrary polarization state in fiber, we would be able to use fibers to transmit polarization-entangled state. That would be great for quantum information transmission.

Task of this experimental-based work is to test and describe properties of polarization-maintaining fibers in notion of laboratory use, propose angular polarization alignment method and try to achieve transmission of arbitrary polarization state.

2

2 Theory

2.1 Polarization

Consider a monochromatic wave of angular frequency ω traveling in the z direction with velocity v. The electric field lies in x-y plane and is described by

$$\mathbf{E}(z,t) = \mathrm{Re}\left\{\mathbf{A}\exp\left[i(\omega t - \frac{z}{v})\right]\right\}, \tag{1}$$

where the complex envelope

$$\mathbf{A} = A_x\mathbf{e_x} + A_y\mathbf{e_y}, \tag{2}$$

is a vector with components A_x and A_y. To describe polarization of this wave we trace the endpoint of the vector $\mathbf{E}$ at each position z as a function of time [1].

Substituting (2) into (1) and expanding to Cartesian basis we obtain parametric equations of polarization ellipse:

$$E_x(z,t) = |A_x|\cos\left[\omega t - \frac{z}{v} + \arg(A_x)\right]$$
$$E_y(z,t) = |A_y|\cos\left[\omega t - \frac{z}{v} + \arg(A_y)\right]. \tag{3}$$

We can rewrite parametric equations (3) into the implicit form of ellipse equation:

$$\left(\frac{E_x}{A_x}\right)^2 + \left(\frac{E_y}{A_y}\right)^2 - 2\frac{E_x}{A_x}\frac{E_y}{A_y}\cos(\delta) = \sin^2(\delta), \tag{4}$$

where $\delta = (\arg(A_y) - \arg(A_x))$ is phase difference [1].

2.2 Jones formalism

Jones formalism is used to describe light in a pure polarization state. Jones vector has the form

$$\mathbf{J} = \begin{bmatrix} A_x \\ A_y \end{bmatrix}, \tag{5}$$

where $\mathbf{J}^\dagger \cdot \mathbf{J} = 1$ and symbol † stands for Hermitian conjugation.

Arbitrary pure polarization state may be described using polarization ellipse and its parameters - *ellipticity* χ and orientation to positive x-semiaxis ψ. Jones vector can be rewritten in notion of elliptical parameters [3]:

$$\mathbf{J}(\psi,\chi) = \begin{bmatrix} \cos(\psi)\cos(\chi) - i\sin(\psi)\sin(\chi) \\ \sin(\psi)\cos(\chi) + i\cos(\psi)\sin(\chi) \end{bmatrix}. \tag{6}$$

Parameters of polarization ellipse are obtained from relation (6) [3]:

$$\psi = \frac{1}{2}\arctan\left[\frac{2\sqrt{A_x A_x^* A_y A_y^*}}{A_x A_x^* - A_y A_y^*}\cos\left(\arg\left(\frac{A_y}{A_x}\right)\right)\right],$$
$$\chi = \frac{1}{2}\arccos\left[A_x^2 + A_y^2\right]. \tag{7}$$

Every environment which changes polarization state, such as polarizers or wave plates, can be described by transformation matrix

$$T = \begin{bmatrix} a_{11} & a_{12} \\ a_{21} & a_{22} \end{bmatrix}, \tag{8}$$

where $a_{ij} \in \mathbb{C}$ for $i, j = 1; 2$.

We describe the transformation matrix of multiple environments $1, 2, \ldots n$ described by matrices $T_1, T_2, \ldots, T_n$ (in order of light propagation) as

$$T = T_n \cdot \cdots \cdot T_2 \cdot T_1. \tag{9}$$

To be more specific, we show transformation matrices which are frequent in use.

The polarizer rotated by an angle α is described by the matrix

$$
\begin{aligned}
POL(\alpha) &= \begin{bmatrix} \cos(\alpha) & -\sin(\alpha) \\ \sin(\alpha) & \cos(\alpha) \end{bmatrix} \cdot \begin{bmatrix} 1 & 0 \\ 0 & 0 \end{bmatrix} \cdot \begin{bmatrix} \cos(\alpha) & \sin(\alpha) \\ -\sin(\alpha) & \cos(\alpha) \end{bmatrix} \\
&= \begin{bmatrix} \cos^2(\alpha) & \cos(\alpha)\sin(\alpha) \\ \cos(\alpha)\sin(\alpha) & \sin^2(\alpha) \end{bmatrix}.
\end{aligned} \tag{10}
$$

The retarder plate which causes phase difference Γ rotated by angle α is described by matrix

$$RET(\alpha)(\Gamma) = \begin{bmatrix} \cos(\alpha) & -\sin(\alpha) \\ \sin(\alpha) & \cos(\alpha) \end{bmatrix} \cdot \begin{bmatrix} 1 & 0 \\ 0 & e^{-i\Gamma} \end{bmatrix} \cdot \begin{bmatrix} \cos(\alpha) & \sin(\alpha) \\ -\sin(\alpha) & \cos(\alpha) \end{bmatrix}. \tag{11}$$

In case of $\Gamma = \pi$ we get the matrix of the half-wave plate

$$HWP(\alpha) = \begin{bmatrix} \cos(2\alpha) & \sin(2\alpha) \\ \sin(2\alpha) & -\cos(2\alpha) \end{bmatrix}. \tag{12}$$

In case of $\Gamma = \frac{\pi}{2}$ we get the matrix of the quarter-wave plate:

$$QWP(\beta) = \begin{bmatrix} \cos^2(\beta) - i\sin^2(\beta) & (1+i)\cos(\beta)\sin(\beta) \\ (1+i)\cos(\beta)\sin(\beta) & -i\cos^2(\beta) + \sin^2(\beta) \end{bmatrix}. \tag{13}$$

Note that we will always use α, β as wave plates angles for the rest of the text.

2.3 Stokes formalism

Stokes formalism is used to describe partially polarized states of light. Every state can be mapped on a sphere of radius r which corresponds to degree of polarization (DOP). If $r < 1$ the light is not in pure state, if $r = 1$ the light is in pure polarization state and the sphere of radius $r = 1$ is called *Bloch sphere* or *Poincare sphere*. The longitude of the point is 2ψ and the latitude is 2χ, where ψ and χ are elliptical parameters of polarized part of light. We see that these elliptical parameters describe pure part of state.

Let x, y, z be Cartesian coordinates of point on sphere. The Stokes vector consists of Stokes parameters:

$$\mathbf{S} = \begin{bmatrix} S_0 \\ S_1 \\ S_2 \\ S_3 \end{bmatrix} = \begin{bmatrix} \sqrt{x^2 + y^2 + z^2} \\ x \\ y \\ z \end{bmatrix} = \begin{bmatrix} r \\ r \cdot \cos(2\psi)\cos(2\chi) \\ r \cdot \sin(2\psi)\cos(2\chi) \\ r \cdot \sin(2\chi) \end{bmatrix}. \tag{14}$$

We define degree of polarization as:

$$DOP = \sqrt{S_1^2 + S_2^2 + S_3^2}. \tag{15}$$

Relation (15) differs from what we can see in literature. Difference is explained in section A.1 in appendix.

Known ellipse parameters ψ, χ could be used as a transition from Stokes to Jones formalism using (6) and from Jones to Stokes using (7) and (14). Due to occurrence of arctan function we are facing $\pi/4$-periodicity problem, so we have to be careful using these relations.

For example, pure state described by Jones vector

$$\mathbf{J}(45°, 22.5°) = \begin{bmatrix} \cos(45°)\cos(22.5°) - i\sin(45°)\sin(22.5°) \\ \sin(45°)\cos(22.5°) + i\cos(45°)\sin(22.5°) \end{bmatrix}, \tag{16}$$

can be expressed as the Stokes vector:

$$\mathbf{J}(45°, 22.5°) \propto \mathbf{S}(45°, 22.5°) = \begin{bmatrix} 1 \\ 0 \\ \frac{1}{\sqrt{2}} \\ \frac{1}{\sqrt{2}} \end{bmatrix}.$$

Figure 4 shows graphical representations of $\mathbf{J}(45°, 22.5°)$ - the polarization ellipse and the Stokes vector.

Main polarization states are defined in Table 1. Every state in the table represents one intersection of Bloch sphere and x, y or z axis. From this point we will use Dirac notation.
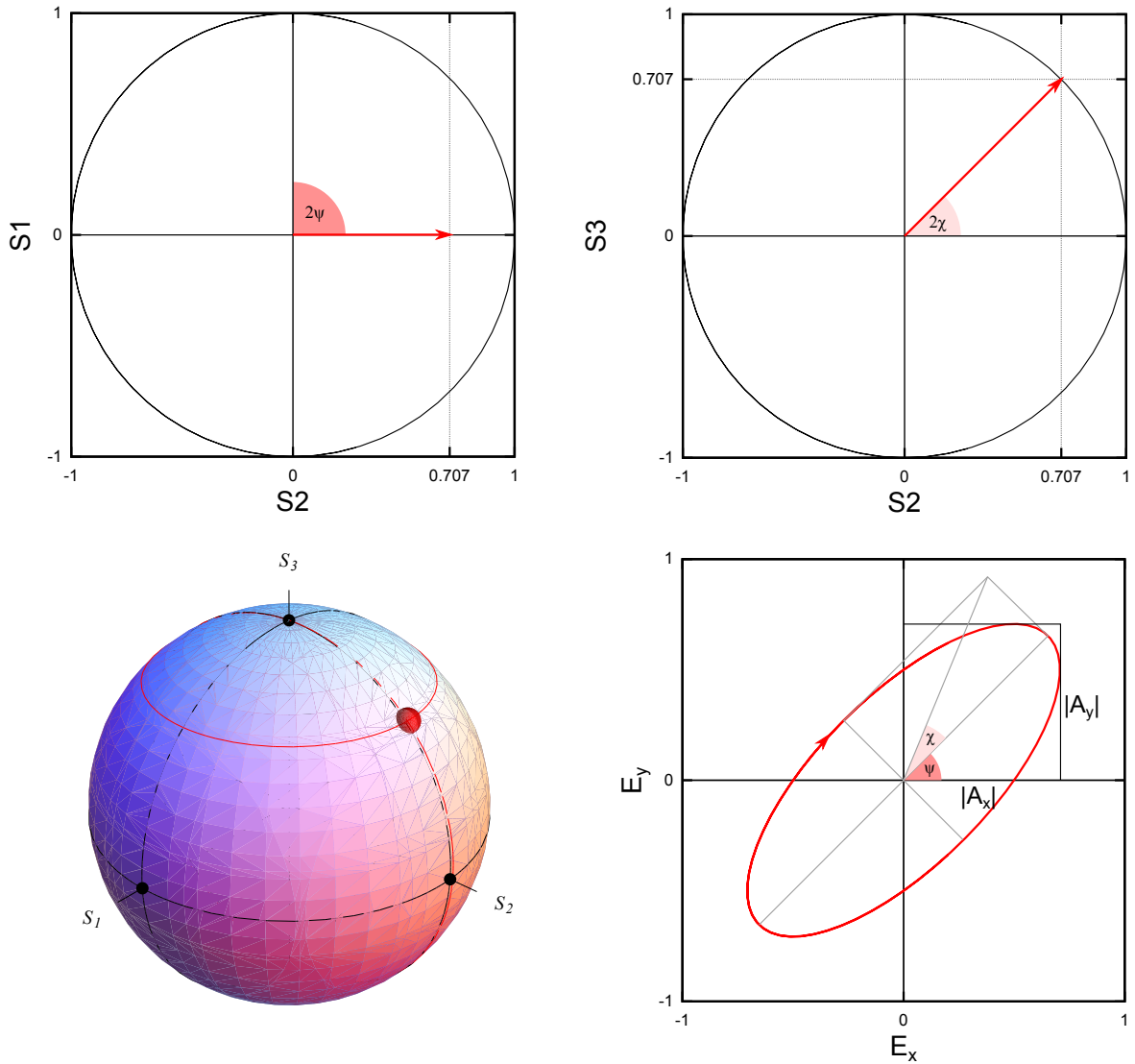
Figure 4: Polarization state expressed as the polarization ellipse and the Stokes vector. Position of positive x'-semiaxis is $\psi = 45°$, ellipticity is $\psi = 22.5°$. Top left and right images show Bloch sphere from top and side. Doubles of angles corresponds with polarization ellipse in the bottom right picture. Bottom left picture shows Bloch sphere from perspective, image was created using [4]. All images represent $\mathbf{J}(45°, 22.5°)$ state.

State name	State ket	Jones formalism	Stokes formalism	Semiaxis position ψ	Ellipticity χ	Ellipse
Horizontal	$|H\rangle$	$\begin{bmatrix} 1 \\ 0 \end{bmatrix}$	$\begin{bmatrix} 1 \\ 1 \\ 0 \\ 0 \end{bmatrix}$	0	0	
Vertical	$|V\rangle$	$\begin{bmatrix} 0 \\ 1 \end{bmatrix}$	$\begin{bmatrix} 1 \\ -1 \\ 0 \\ 0 \end{bmatrix}$	90	0	
Diagonal	$|D\rangle$	$\frac{1}{\sqrt{2}}\begin{bmatrix} 1 \\ 1 \end{bmatrix}$	$\begin{bmatrix} 1 \\ 0 \\ 1 \\ 0 \end{bmatrix}$	45	0	
Antidiagonal	$|A\rangle$	$\frac{1}{\sqrt{2}}\begin{bmatrix} 1 \\ -1 \end{bmatrix}$	$\begin{bmatrix} 1 \\ 0 \\ -1 \\ 0 \end{bmatrix}$	-45	0	
Right-circular	$|R\rangle$	$\frac{1}{\sqrt{2}}\begin{bmatrix} 1 \\ i \end{bmatrix}$	$\begin{bmatrix} 1 \\ 0 \\ 0 \\ 1 \end{bmatrix}$	-	45	
Left-circular	$|L\rangle$	$\frac{1}{\sqrt{2}}\begin{bmatrix} 1 \\ -i \end{bmatrix}$	$\begin{bmatrix} 1 \\ 0 \\ 0 \\ -1 \end{bmatrix}$	-	-45	
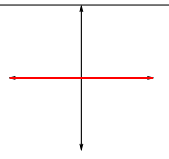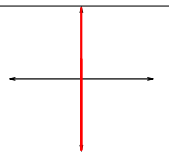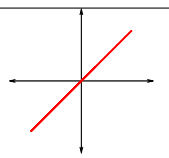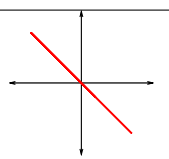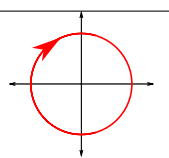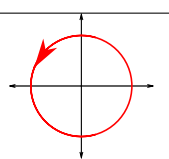
Table 1: Table of main states in both formalism. States are expressed in Dirac notation as kets.

2.4   Preparation of polarization state and projection to state.

Our experiment setup uses polarizer (POL), half-wave plate (HWP) and quarter-wave plate (QWP) (in direction of light propagation) to prepare an arbitrary polarization state.

Preparation of state $|J_{out}\rangle$ from initial $|H\rangle$ polarization state requires knowledge of wave plates setting angles α, β. We can get wave plates setting by solving equation

$$QWP(\beta)HWP(\alpha)|H\rangle \;=\; |J_{out}\rangle. \tag{17}$$

Projection is a symmetric problem. We use QWP, HWP and POL to measure projection of input state to state $|J_{proj}\rangle$. To obtain wave plates setting we solve:

$$HWP(\alpha)QWP(\beta)|J_{proj}\rangle \;=\; |H\rangle. \tag{18}$$

The most convenient solutions of equations (17) and (18) are in Table 2.

State	Preparation of HWP $\alpha[°]$	Preparation of QWP $\beta[°]$	Projection to HWP $\alpha[°]$	Projection to QWP $\beta[°]$
$|H\rangle$	0	0	0	0
$|V\rangle$	45	90	45	90
$|D\rangle$	22.5	45	22.5	45
$|A\rangle$	-22.5	-45	-22.5	-45
$|R\rangle$	-22.5	0	22.5	0
$|L\rangle$	22.5	0	-22.5	0

Table 2: The most convenient solutions of (17), (18) for states from Table 1.

2.5   Tomography and polarization state reconstruction

We will use direct reconstruction method of polarization analysis. Every state can be described as a mixture of pure states, the density matrix is suitable for describing such mixtures. Measured intensities give us information about mean values of density matrix (which describes mixed states) with respect to given base. These mean values represents probability of finding state in given projection. We can write it in form of equations:

$$\langle H|\hat{\rho}|H\rangle = \rho_H = \frac{I_H}{I_H + I_V},$$
$$\langle D|\hat{\rho}|D\rangle = \rho_D = \frac{I_D}{I_D + I_A}, \tag{19}$$
$$\langle R|\hat{\rho}|R\rangle = \rho_R = \frac{I_R}{I_R + I_L},$$

where $\hat{\rho}$ is the density matrix which can be expanded to sum of Pauli's matrices ($S_0 = 1$ for pure polarization state):

$$\rho = \frac{1}{2}\sum_1^3 (S_i \sigma_i) = \frac{1}{2}\left(\begin{bmatrix} 1 & 0 \\ 0 & 1 \end{bmatrix} + S_1 \begin{bmatrix} 1 & 0 \\ 0 & -1 \end{bmatrix} + S_2 \begin{bmatrix} 0 & 1 \\ 1 & 0 \end{bmatrix} + S_3 \begin{bmatrix} 0 & -i \\ i & 0 \end{bmatrix} \right).$$

By solving (19) we obtain components of the Stokes vector:

$$S_1 = \frac{2I_H}{I_V + I_H} - 1,$$
$$S_2 = \frac{2I_D}{I_D + I_A} - 1,$$
$$S_3 = \frac{2I_R}{I_R + I_L} - 1, \tag{20}$$
$$S_0 = \sqrt{S_1^2 + S_2^2 + S_3^2}.$$
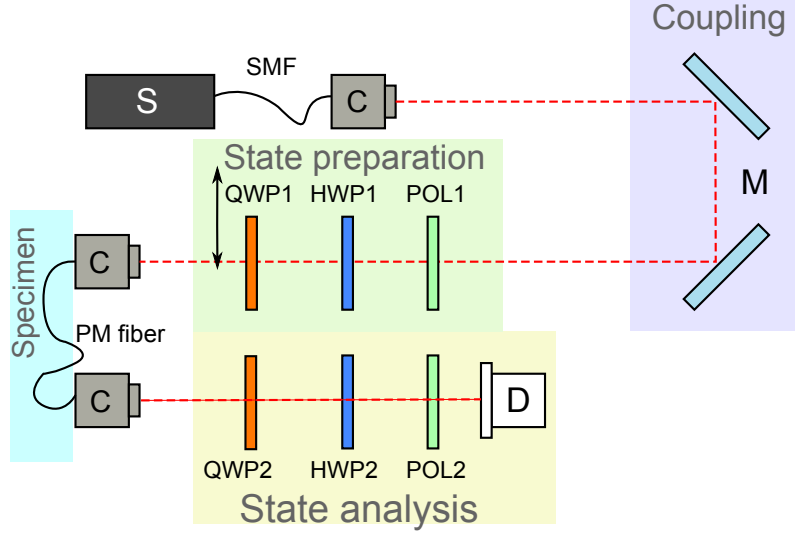
3 Experiments

3.1 Setup

Figure 5: Scheme of core-setup: S - laser source; SMF - single mode fiber; C - collimator; M - pair of mirrors; POL1 - H-polarizer; HWP1 - half-wave plate; QWP1 - quarter-wave plate; PM fiber - polarization-maintaining fiber specimen; QWP2 - quarter-wave plate, HWP2 - half-wave plate; POL2 - H-polarizer; D - detector.

Scheme of core-setup is shown in Figure 5. The light from laser diode S propagates through the single mode optical fiber (*SMF*, Thorlabs 780HP) and then it is decoupled by collimator C (Schäfter + Kirchhoff 60F-011-02, focal length 11mm). Mirrors M are used to couple beam into fiber.

To set linear polarization of the beam the polarizer (LP VIS 050) is used. The polarization state is prepared using the half-wave plate (*HWP*, Eksma 810nm) and the quarter-wave plate (*QWP*, Eksma, 810nm). QWP1 has not been used sometimes - to emphasize that fact we put the double-arrow symbol next to QWP1 in scheme.

The beam is coupled by collimator (Schäfter + Kirchhoff 60F-011-02) into the tested polarization-maintaining fiber (*PM fiber*). Then it is decoupled from collimator (Thorlabs F220FC-B).

The polarization of light is analyzed using method described in section 2.5. We use QWP2 (Eksma, wavelength 810nm), HWP2 (Eksma, wavelength 812nm) and polarizer (Thorlabs LP VIS 050) to project polarization state into one of measured states. Wave plates are mounted on motorized stages (Newport PR50) controlled by a RS232 controllers (Newport SMF100CC) in order to make measurement more convenient. Beams ends in detector D. We used the PIN diode (Thorlabs DET36A/M) or the Fieldmaster detector (Coherent) to detect intensity. The PIN diode represents measured intensity as a voltage. We plugged output voltage via variable resistor to the multimeter (Aim&TTi 1906). Fieldmaster detector was connected to LM-2 VIS detector head. See section A.6 for list of used parts.

3.2 Used alignment method

Polarization-maintaining fiber is designed to maintain a linear polarization in direction of slow or fast axis. Coupled light has to be linearly polarized in direction of fast or slow axis.

We had tried alignment method described in article [5]. The method is based on heat-inducing birefringence in the PM fiber and observing changes in polarization at the output of PM fiber - the smaller changes, the better alignment. It had not been efficient enough because of polarization mode dispersion in PM fiber as we will mention later. We believe that for sources with larger coherence length would this method worked better. The coherence length of our laser was in order of $80\,\mu\mathrm{m}$.

That is why we were using DOP-based alignment method. Polarization modes in PM fiber have different velocities due to anisotropy of PM fiber. It causes dispersion of polarization modes which acts as DOP losses. When the wave is propagating exclusively in one of preferred modes, the dispersion effects are significantly weaker and as a result DOP losses are low. This is naively depicted in Figure 6. Term *DOP-alignment* means preparation of such polarization states.
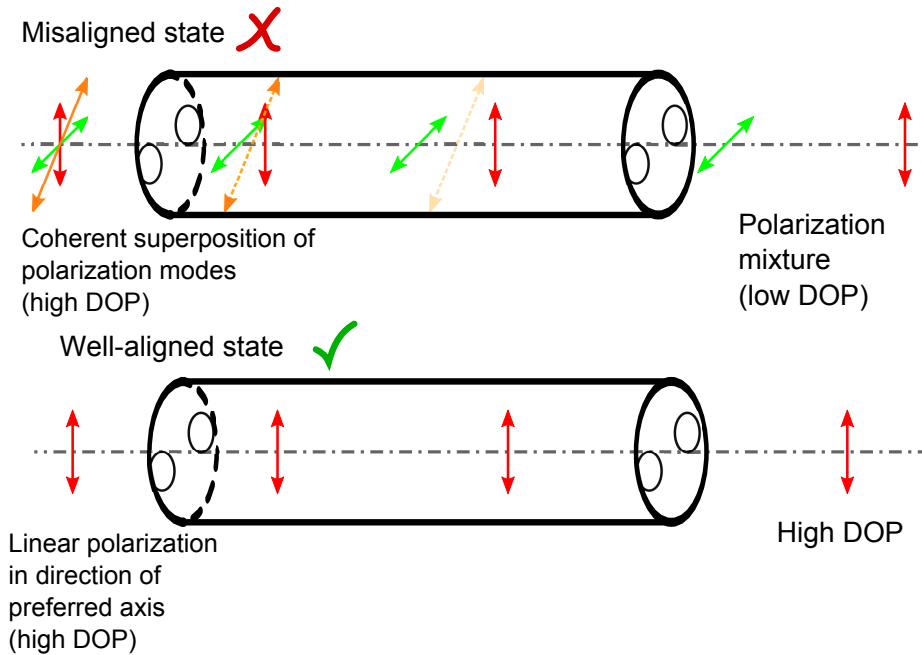
Figure 6: Naive explanation of idea behind DOP-based alignment. In case of misaligned state the distance of wave packets exceeds coherence length - therefore polarization components at the output are not coherent. This acts as low DOP. Well-aligned state propagates exclusively in one polarization mode. The output state is coherent and as a result we can measure high DOP.

DOP measurement after each change of input polarization would make this method very slow as fast polarimeter was not available. Tomography analysis would take us too long. One measurement of DOP took about half minute in our setup.

We made following assumption: If there is a well-aligned state at the PM fiber input, the output state is linear.

From knowledge of orientation of PM fiber output preferred axis θ we can maximize DOP by minimizing projection to $|\theta + 90°\rangle$ state.

We can estimate angular position θ of PM fiber axis at the output side of fiber. By minimizing projection to perpendicular $|\theta + 90°\rangle$ state we can maximize amount of energy in one axis and thus maximize DOP.

We use QWP1 and HWP1 on the input to prepare well-aligned state, and QWP2 and HWP2 to project to $|\theta + 90°\rangle$. See Figure 8 how to use this DOP-alignment method step-by-step.

Proposed method works well - about 99% of DOP achieved in few minutes. One thing concerned us: In early stages of experiment we have realized that QWP1 was needed to achieve high DOP even we would think that HWP1 is enough. Something changed linear polarization to elliptical - and this ellipticity had to be compensated using QWP1, see Figure 7. We will discuss the need for QWP1 later.
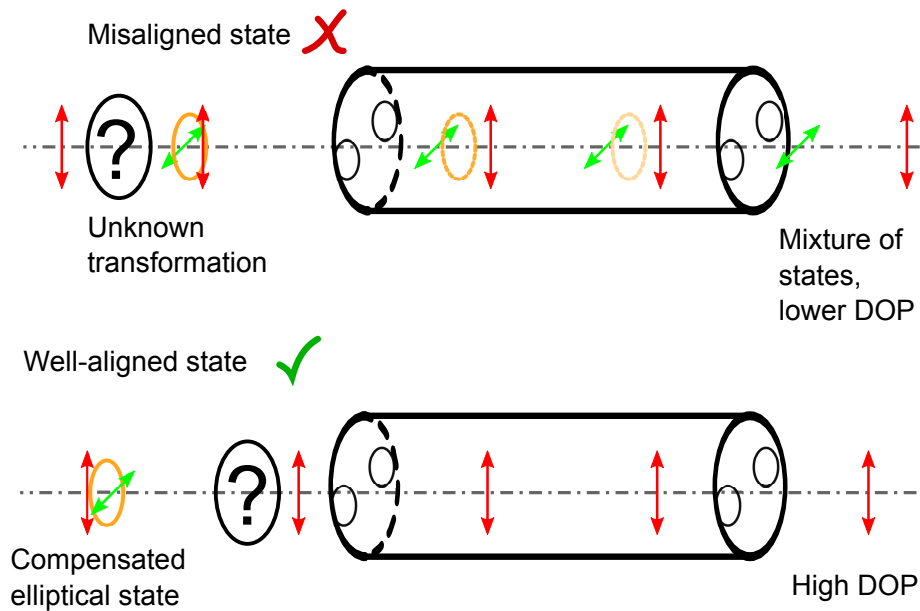
Figure 7: The unknown transformation adds ellipticity to input state and creates misaligned state. Using QWP1 it is possible to compensate ellipticity caused by the unknown transformation and achieve well-aligned state.
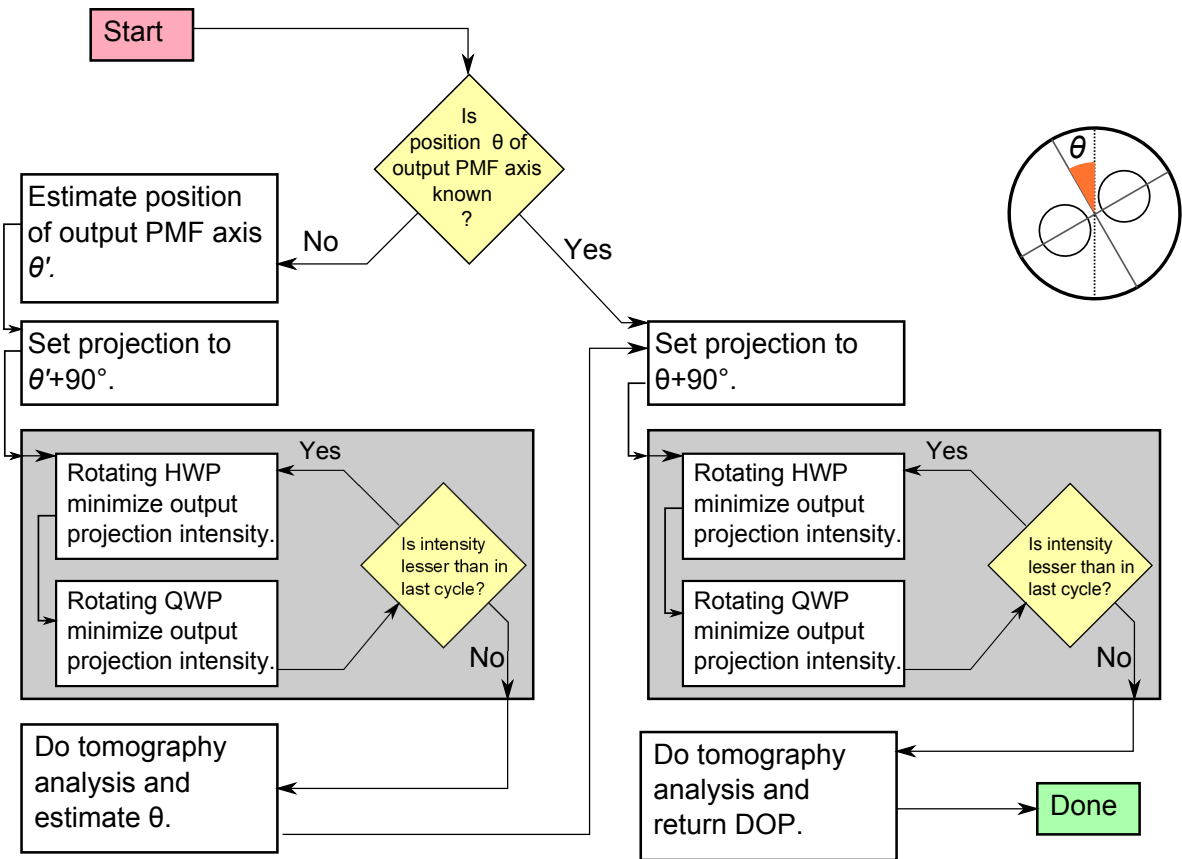
Figure 8: Flowchart shows DOP-alignment method. PMF stands for PM fiber.

3.3 Setup stability

Standard law of error propagation can not cover all influences that come from the nature of tomography measurement. We wanted to know how stable and repeatable is our measurement.

That is why we did DOP time stability test. Series of measurement was performed to determine how DOP changes in time. The test was done for well-aligned state at the input.

One measurement cycle took 28 s. The mean value and standard deviation was $DOP \approx (0.9986 \pm 0.0003)$. Measured data are represented by Figure 9. We see that setup was sufficiently stable.
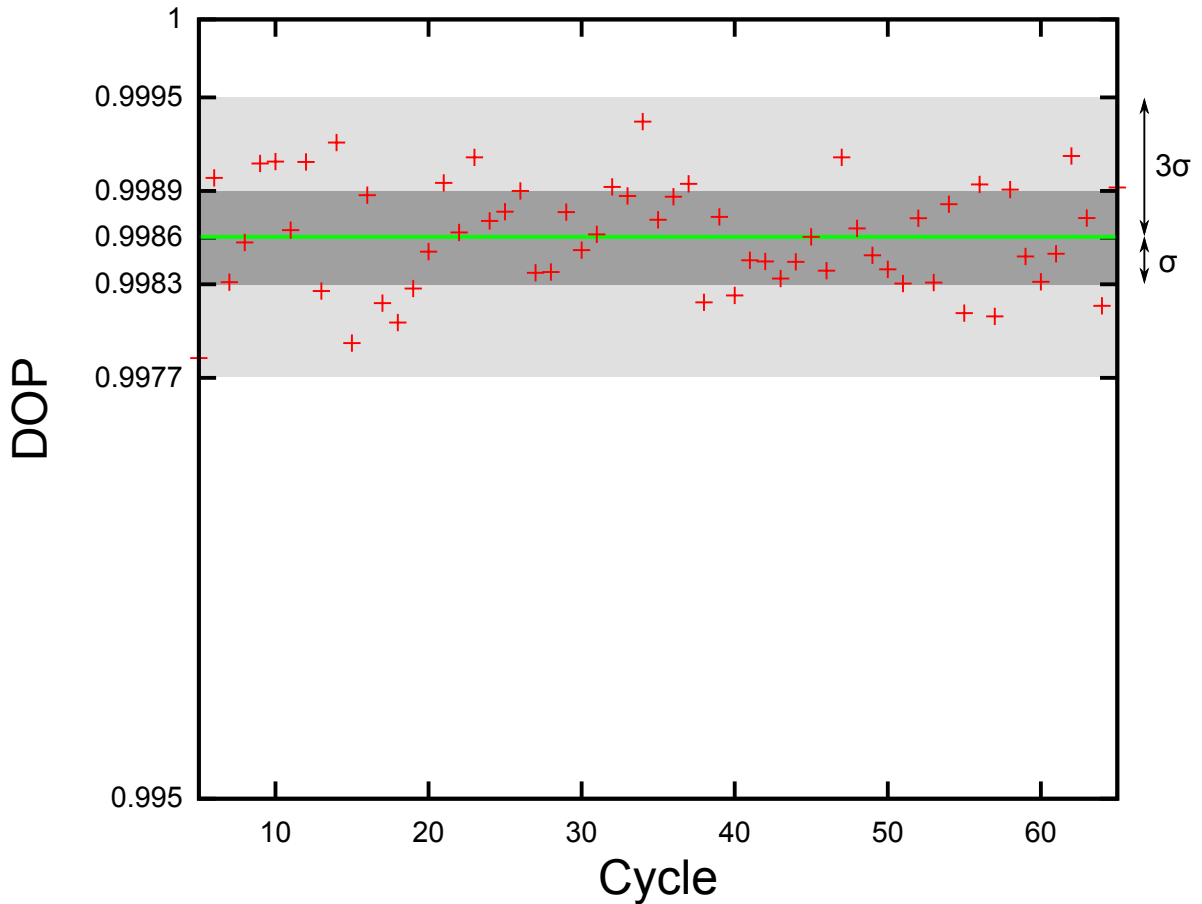
Figure 9: DOP stability in time. DOP = (0.9986 ± 0.0003). Green line represents mean value, dark gray area represents interval of $\pm\sigma$, gray area represents interval $\pm 3\sigma$.

3.4 DOP scan

Purpose of this experiment was to verify the DOP-based alignment method and explore how use of the QWP1 affects DOP at the output. We used OZ Optics t1607821-2 as the PM fiber specimen. At first, we used HWP1 only to align input polarization into PM fiber. We were curious what is the maximal DOP we can get. Our script rotated HWP1 from 0° to 360° with step 0.5° and measured DOP in each point, as depicted in Figure 10. Maximal DOP was $DOP = (0.864 \pm 0.001)$ at HWP angle $\alpha = 114°$ which corresponds to linear polarization with

14

direction $\psi \approx 48°$. The output Stokes vector at this point was

$$\mathbf{S} = \begin{bmatrix} 0.864 \pm 0.001 \\ -0.852 \pm 0.001 \\ -0.142 \pm 0.002 \\ 0.014 \pm 0.003 \end{bmatrix}.$$
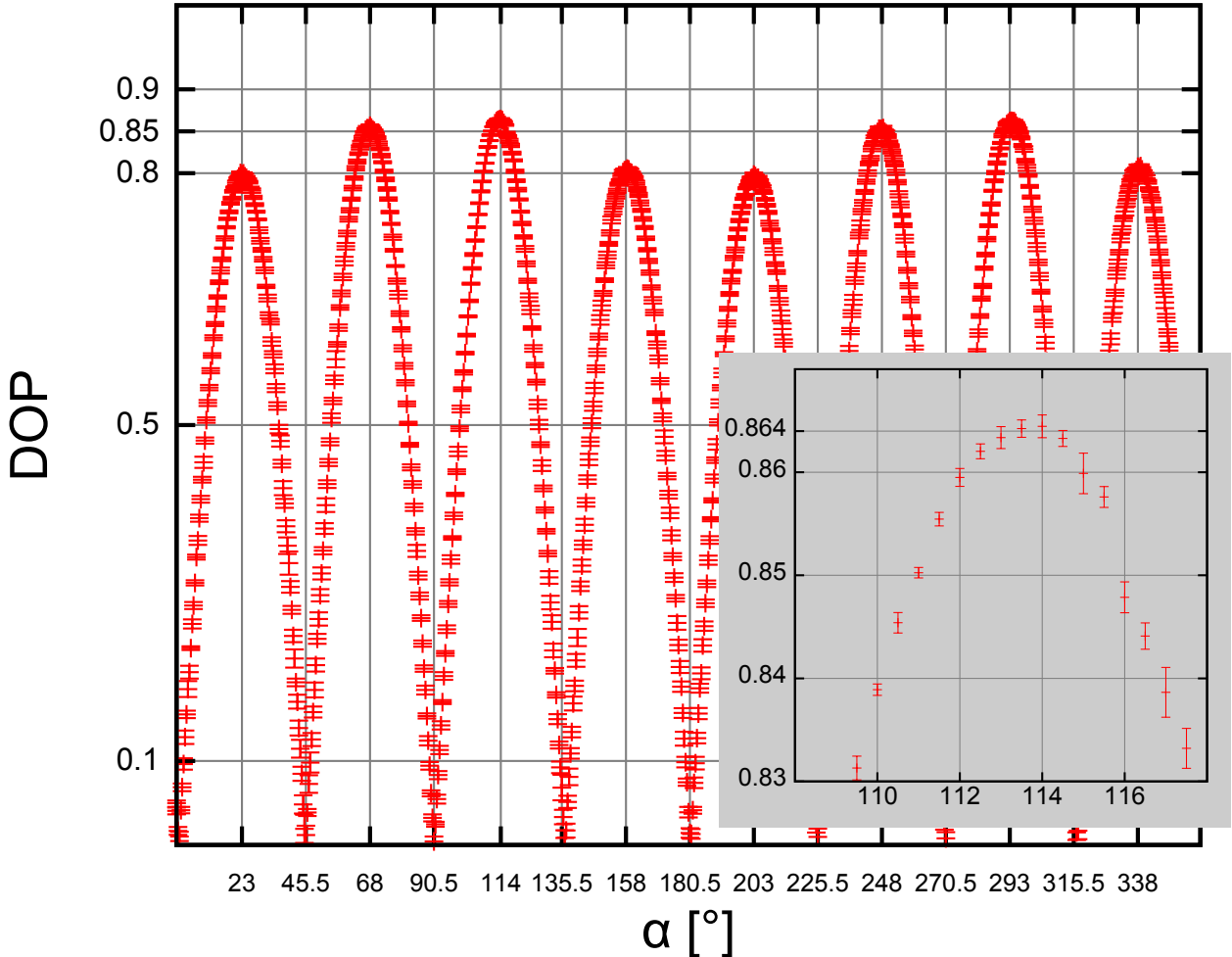
Figure 10: Dependence of DOP on HWP1 rotation. QWP1 was not present in preparation part of setup. Error bars represent deviations of 1σ. Inset contains close-up of maximal DOP area. We can also see that peaks are not equally high.

We put the QWP1 back into setup in order to see if we could get higher DOP. Scan of various combinations of QWP1 and HWP1 angles was performed. Figure 11 shows dependence of DOP on wave plates angles α, β. We see that presence of QWP1 does matter - the improvement was 13.5% of DOP. Peaks of scanned surface are in Table 3.

Polarization ellipses of input states calculated using Jones formalism and wave plate setting are plotted in Figure 12.

15

$\alpha[°]$	$\beta[°]$	DOP [%]	$\sigma[\%]$	$\psi[°]$	$\chi[°]$	$\delta[°]$
123	46	99.9	0.2	46	-20	-40
77	45	99.23	0.01	-45	19	142

Table 3: Scan peaks table shows input wave plates setting, corresponding polarization ellipse parameters and the output DOP. The value σ is standard deviation of DOP.
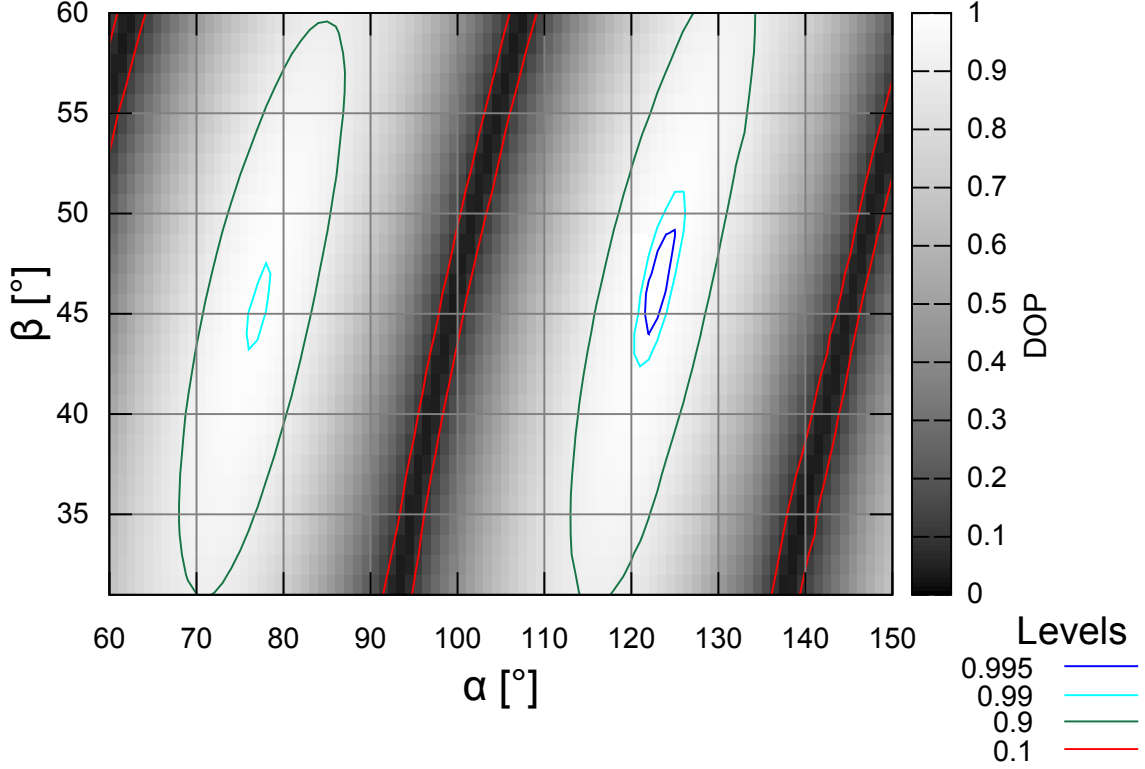
Figure 11: Scan results shown as height map. The horizontal axis represents HWP angle, the vertical axis represents QWP angle. The DOP values are mapped in grayscale - black stands for zero, white for one. Certain levels of interest are highlighted by colored curves.

To conclude this section: Our DOP-based alignment method works sufficiently. We can also see that proper DOP-alignment of polarization depends on presence of QWP1, because output DOP is dependent also on input ellipticity. At this point we were facing new question - what causes the need for ellipticity compensation?
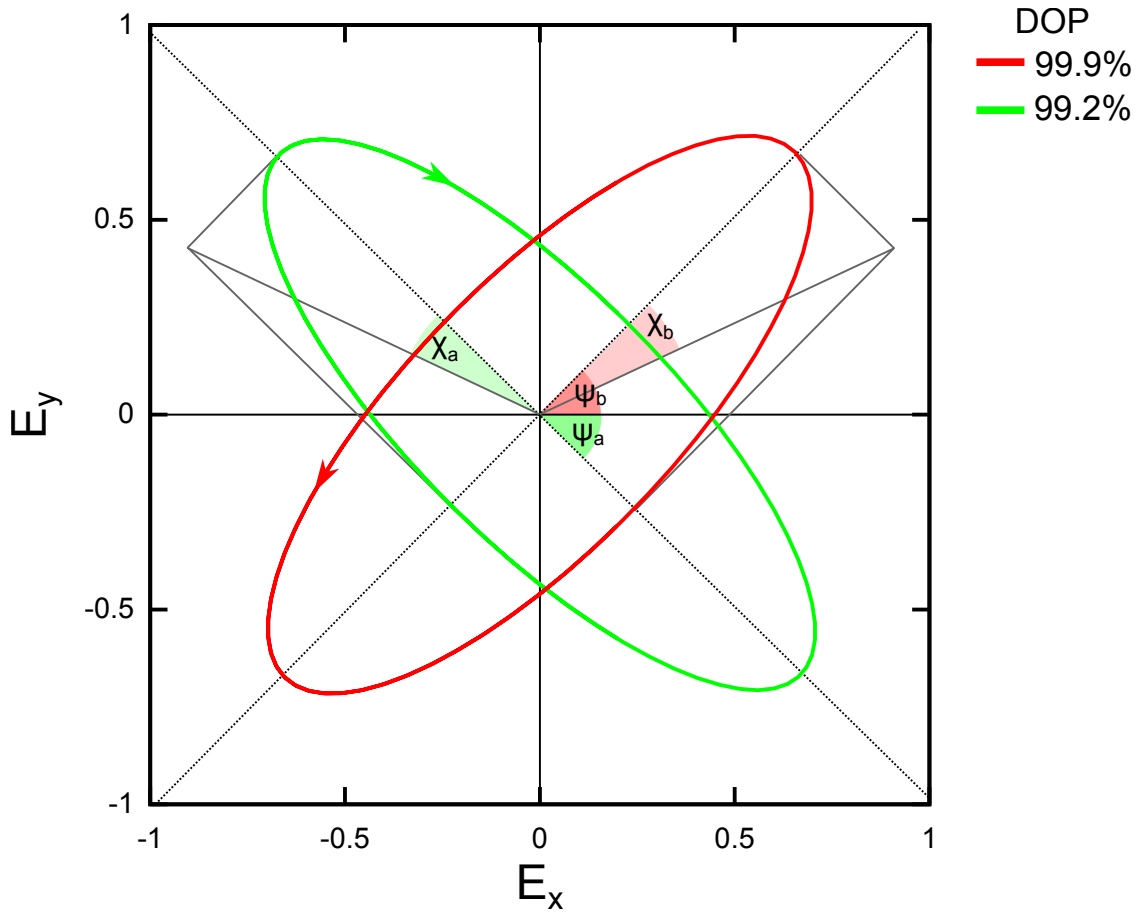
Figure 12: Figure shows theoretical input states which had maximal DOP. Calculation was based on Jones calculus and measured DOP. $\psi_a = -45°$, $\chi_a = 19°$, $\psi_b = 46°$, $\chi_b = -20°$. Absolute value of states inner product is $|\langle A_{green}|B_{red}\rangle| \approx 0.0349$. It represents orthogonality of polarized parts of states, the closer to zero is inner product, the more orthogonal polarized parts of states are. We consider states quite orthogonal. We expected this result because axes of PM fiber are orthogonal too. Reader may notice that both axes of tested PM fiber have good DOP transmission.

3.5 Maximal DOP with and without QWP1 - various PM fibers

We assume that mechanical stress within the PM fiber connector causes additional birefringence and therefore need for input ellipticity compensation. We measured 10 PM fibers made by OZ Optics, 5 by SQS and two PM couplers which will be discussed later. We were interested in difference between maximal output DOP using HWP1 only and using HWP1 plus QWP1.

During this measurement we were using the DOP-alignment method which was discussed in section 3.2. HWP1 and QWP1 were placed in manual mounts. As we were interested in DOP during the measurement, not input states, we do not know real angles of HWP1 and QWP1, we know just angles of mounts. Table 4 shows representative results, complete data is provided in appendix - see Table 16.

Manufacturer	ID	Max. DOP with QWP [%]	Max DOP without QWP [%]	Note
OZ Optics	t16078212	100.0 ± 0.3		Best DOP.
	t16078412	99.77 ± 0.02	87.13 ± 0.05	Typical value.
SQS	0100728719	99.74 ± 0.03	89.18 ± 0.04	Best DOP without QWP for single fiber.
	0100728718	99.78 ± 0.02	86.8 ± 0.2	Typical value.
Canadian Instrumentation	68933VRCPM	99.40 ± 0.2	97.3 ± 0.2	
	68933VRCPM	99.6 ± 0.3	84.3 ± 0.3	

Table 4: Highlights from PM fibers measurement results. Only common or interesting values were shown.

DOP scan revealed that well-aligned states have non-zero input phase difference. In other words: DOP of the output state depends on the input phase difference. We would like to see how much input phase difference δ differs from one specimen to another.

As we do not know real angles of HWP1 and QWP1 we are not able to express theoretical input states. But we can use mount angles to calculate "measure of phase difference similarity" μ using the Jones formalism. The "measure of similarity" could be used to compare input states to each other and quantify their similarity. μ is calculated same way as phase difference from Jones vector and therefore it has relation to phase difference. We would like to emphasize that Jones vector calculated from HWP1 and QWP1 mount angles does not represent a real state - it is just a tool for comparing phase difference of states.

In order to avoid periodicity-related problems we applied normalization

$$N(\mu) = \begin{cases} \arccos(\cos(\mu)) & \mu \in \left(0 + 2k\pi; \frac{\pi}{2} + 2k\pi\right) \\ -\arcsin(\sin(\mu)) & \mu \in \left(\pi + 2k\pi; \frac{3\pi}{2} + 2k\pi\right) \end{cases}, \tag{21}$$

where $k \in \mathbb{Z}$. It maps angles from both k-periodic quadrants to first quadrant ($k = 0$).

μ of well-aligned states was $\mu_{OZ} = (58 \pm 2)°$ in case of OZ Optics. For SQS fibers it was $\mu_{OZ} = (59 \pm 2)°$. We see that μ does not differ much for both OZ Optics and SQS manufacturer. In other words: phase differences of well-aligned input states are very similar.

It seems that various PM fibers need very similar additional ellipticity compensation at the input. This is in contradiction with assumption that fibers do not have uniform stress in their connectors. Therefore stress within the connector and its effect on input polarization state could be neglected.

3.6 PM variable ratio evanescent wave couplers

Another point of our interest was characterization of PM coupler. We would like to answer following questions: How splitting ratio affects maximal DOP at the output? Is the output DOP same at both outputs?

We have tested two PM couplers made by Canadian Instrumentation, nowadays known as Evanescent Optics Inc. PM coupler was plugged as a fiber specimen in our setup. The scheme of PM coupler is shown at Figure 13.

Principle of operation is explained by manufacturer:
"Variable ratio couplers are made with optically contacted polished fibers mounted in substrate blocks that have transverse motion in the contact plane to adjust core-to-core separation distance. In the case of PM fiber, the orientation of the fast and slow axes is preserved during the motion. A negligibly thick oil layer is used to lubricate the substrate blocks and ensure smooth motion. Fine transverse motion is accomplished by means of a micrometer and lever system." [7]
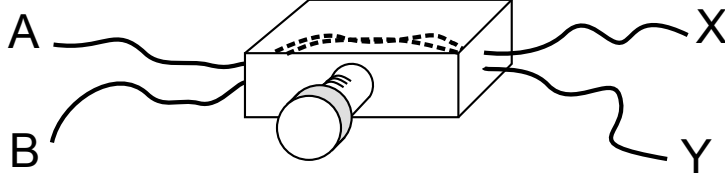
Figure 13: Scheme of PM coupler. We have two input PM fibers labeled as A and B. We can regulate level of contact using a micrometer screw system. At the output there are two fibers labeled as X and Y.

Results in Table 5 shows DOP for various coupling ratio. DOP-alignment was done in two different ways - the first used both HWP1 and QWP1, the second used HWP1 only.

ID	In	Out	Ratio X:Y	Max. DOP [%] using QWP1 and HWP1	Max. DOP [%] using HWP1 only
68933	A	Y	50:50	98.84 ± 0.07	96.6 ± 0.1
	A	X	50:50	98.9 ± 0.1	98.15 ± 0.09
	A	X	100:0	99.1 ± 0.1	94.4 ± 0.2
	A	Y	0:100	99.0 ± 0.3	96.83 ± 0.09
	A	X	45:20	99.4 ± 0.2	97.3 ± 0.2
68932	B	Y	100:0	99.8 ± 0.2	84.2 ± 0.1
	B	Y	33:66	99.6 ± 0.3	84.3 ± 0.3
	B	X	50:50	98.80 ± 0.08	83.7 ± 0.1
	B	Y	50:50	99.0 ± 0.1	84.3 ± 0.1

Table 5: Results of PM variable coupler. We measured maximal DOP for various splitting ratios.

Measured data reveals that DOP of well-aligned state is not very sensitive on splitting ratio. The specimen 68932 acts more like previously measured PM fibers - presence of QWP increased DOP by 15.2% in average.

3.7 Coupling lenses and DOP-alignment.

Coupling lens could affect input polarization state. Each test of lens consisted of coupling the beam into PM fiber via tested collimator, DOP-alignment using HWP only and DOP

measurement. Results are in Table 6.

Due to some organization and technical reasons the experimental setup was changed slightly. QWP2 and HWP2 were mounted into manual mounts, Fieldmaster detector was replaced by Thorlabs PIN diode + multimeter Aim&TTi 1906 and polarizers POL1 and POL2 were set crossed (before changes they were parallel). Projection angles from Table 2 had to be modified. As the fiber specimen was used OZ Optics t1607821-2.

Results in Table 6 reveals that major part of unwanted phase difference was caused by used lens. This explains the need for ellipticity compensation in DOP-alignment. The "unknown" transformation from section 3.2 is "not that unknown" anymore.

We realized that if input collimator changes polarization, the output collimator could change polarization too. DOP-alignment flowchart was modified to take output collimator effect into account, see Figure 23 in appendix.

Manufacturer	ID	DOP	Note
Schäfter+Kirchoff	First used, S/N n.a.	86.33 ± 0.02	From previous results.
	S/N: 000670	66.89 ± 0.03	
	S/N: 000671	95.17 ± 0.01	
	S/N: 000672	84.75 ± 0.03	
	S/N: 000681	83.32 ± 0.03	
	S/N: 000692	97.725 ± 0.004	
	S/N: 000693	99.895 ± 0.007	
	S/N: 000702	99.80 ± 0.02	
VOD	S/N: n.a.	99.58 ± 0.02	

Table 6: The highest DOP achieved using HWP1 only for various coupling collimators. The coupling lens has a major effect on single-HWP achieved DOP.

3.8   DOP vs. deformation

The next thing we were curious about is deformation-induced DOP loss. We used two cylinders of different size to bend tested PM fiber. Then we made a tomography analysis to determine DOP. We did this analysis for DOP-alignment with and without QWP1. We would expect that well aligned polarization is rather insensitive to bend deformations of fiber. See Table 7 and 8 for measured values.

As a result we see that well-aligned input polarization is resistant to PM fiber bending deformation, just as we expected.

Bend diameter [mm]	Turns	DOP with QWP [%]
-	-	99.40 ± 0.02
32	5	99.36 ± 0.03
32	10	99.34 ± 0.02
32	15	99.33 ± 0.05
60	8	99.35 ± 0.03

Table 7: DOP vs. deformation of PM fiber. We can observe that deformation has only a little effect on output DOP. Measurement was performed on PM fiber OZ Optics t1607831-1.

Bend diameter [mm]	Turns	DOP without QWP [%]
-	-	87.9 ± 0.1
32	5	88.0 ± 0.1
32	7	87.8 ± 0.3
60	4	86.5 ± 0.6

Table 8: Table reveals that misaligned states are more sensitive to deformation. Measurement was performed on PM fiber OZ Optics t160721-2.

3.9   Series of PM fibers

Another important criteria for choosing the best manufacturer is precision of key-to-axis alignment. It is possible to quantify this property as dependence of DOP loss on number of PM fibers connected in series.

We made DOP-alignment and measured DOP for one PM fiber. Then we were adding more PM fibers and repeating the cycle. We ended with 5 PM fibers connected into "chain". "Chain" consisted of two pieces of 1m long PM fibers, one piece of 2m PM fibers and two pieces of 3m long PM fibers. This measurement was performed for PM fiber made by following manufacturers: OZ Optics, SQS and Optokon.

From Table 9 and graph in Figure 14 we can see that more connected fibers means lower DOP. We assume that DOP losses are caused by PM fiber axes misalignment at each connection. OZ Optics and SQS have acceptable amount of DOP losses. Dependence of DOP on the combination of connectors was observed at PM fibers by Optokon.

Manufacturer	Number of PM fibers	DOP [%]	σ [%]	Note
OZ Optics	1	99.63	0.02	
	2	97.81	0.03	
	3	96.13	0.02	
	4	94.86	0.04	
	5	94.64	0.02	
SQS	1	99.57	0.01	
	2	97.722	0.007	
	3	96.762	0.005	
	4	95.360	0.008	
	5	95.208	0.009	
Optokon	1	99.64	0.02	First try.
	2	94.72	0.01	
	3	90.36	0.02	
	4	73.61	0.15	
	5	49.8	0.1	
	1	99.584	0.006	Second try:
	2	96.68	0.02	with different
	3	96.86	0.03	2m PM fiber piece.
	4	69.93	0.02	
	5	67.10	0.03	
	1	99.70	0.01	Third try.
	2	91.858	0.009	
	3	91.76	0.02	
	4	80.43	0.07	

Table 9: DOP loss dependence on number of PM fiber connected in series. All data (except last one) were obtained at same configuration. First (1,2) were connected two 1 m long fibers, then (3) one fiber of length 1 m and at last (4,5) two 3 m long fibers. Total length of PM fiber series was 10 m.
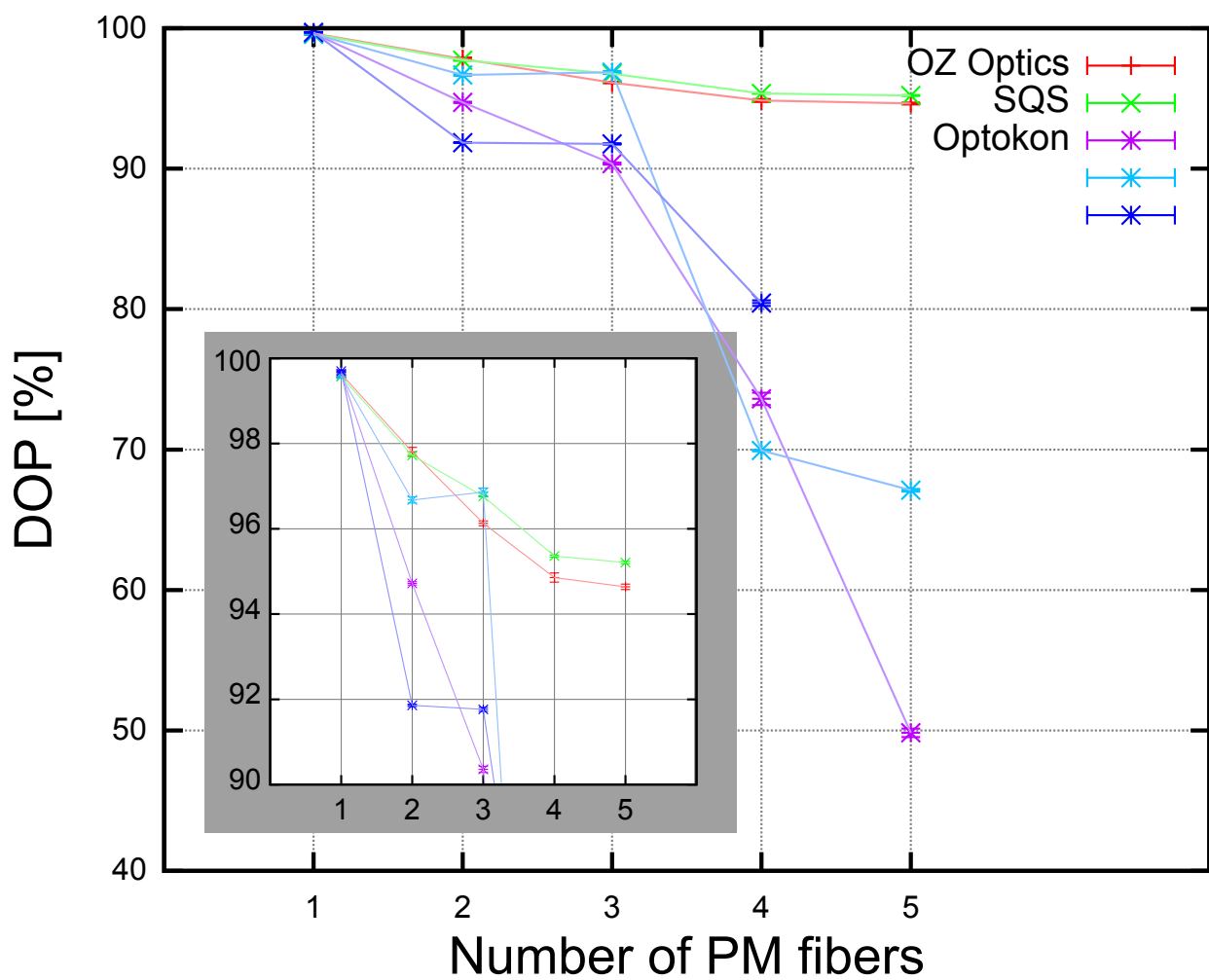
Figure 14: DOP dependence on number of PM fibers in series. We see that DOP is decreasing by adding more PM fibers. Error bars show standard deviation of 1σ, deviations are too small to be clearly visible.

3.10 Transmission of arbiratry polarization state by PM fiber

PM fibers are designed to maintain linear polarization only. One of our task was to overcome this limitation. As we have discussed in section 3.2, the decoherence in PM fiber (therefore DOP loss) was caused by different velocities of polarization modes. Therefore we need to compensate this difference. We propose to connect two PM fiber of same length with crossed axes - the fast axis of first fiber should match the slow axis of the second one, as naively illustrated in Figure 15 (compare with Figure 6). We will call this special type of connection a *cross-connection*. As a result, polarization components should meet each other at the end of the second fiber.
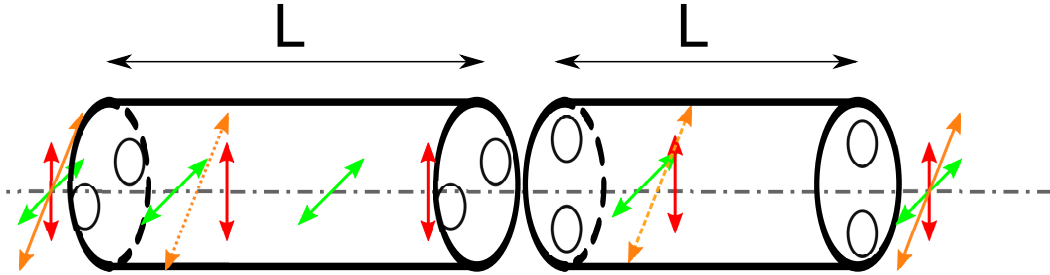

Figure 15: Naive explanation of a cross-connection. We have cross-connected PM fibers of same length *L*. Polarization component in fast axis is traveling faster than in slow axis. As a result the distance between polarization components exceeds coherence length at the end of first fiber. But in the second fiber they will swap velocities and at the end of the second fiber they meet each other. Output polarization components maintains in a coherent superposition.

Testing of proposed method consistes of sending states through cross-connected PM fibers and their polarization analysis. First we DOP-aligned state into the first PM fiber. Well-aligned state was considered as $|H'\rangle$ state. We used knowledge of input wave plates setting to prepare input states $|V'\rangle$, $|D'\rangle$, $|A'\rangle$, $|R'\rangle$ and $|L'\rangle$ which we were sending through cross-connected fibers. Details about these input state are in Table 15 in appendix. We tested three cross-connection implementations: *the welded cross-connection*, *the special connector* and *the cross-mating sleeve*.

At Optokon R/D department was made a special PM fiber by welding two pieces of PM fiber rotated to each other by 90 degrees. The advantage was that cross-connected fibers were in one piece without any movable parts. The disadvantage was however low mechanical resistance - welded join was fragile due to presence of stress-members. We observed higher attenuation, the intensity measure was approximately at 60% of single fiber *intensity measure*. The *intensity measure* is calculated as sum of six tomography projection intensities. It was used ad-hoc to extract additional information from existing raw data. Next disadvantage is complicated manufacturing process.

All states propagated with DOP higher than 94%. However there was unwanted ellipticity changes in states that were not aligned in preferred axes. We assume that major part of unwanted ellipticity was caused by unequal length of cross-connected PM fibers. Minor part

of unwanted ellipticity migh be caused by decoupler collimator lens and fast-to-slow axes misalignment.

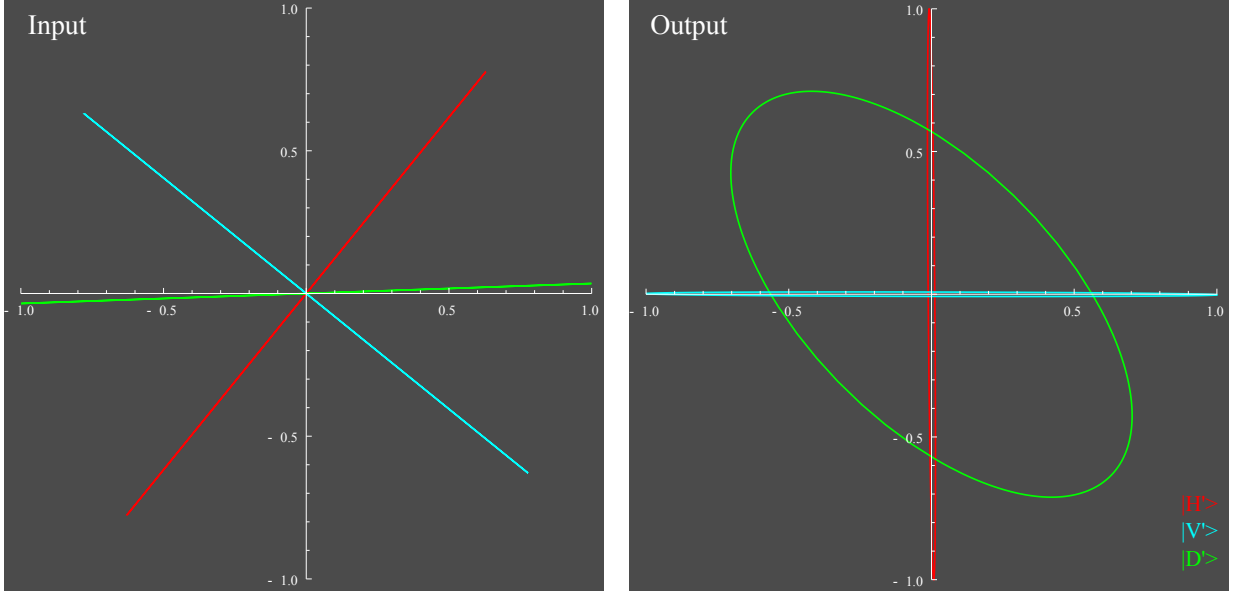Figure 16 shows tested states before and after propagation. Data are in Table 10.

Figure 16: Welded cross-connection implementation. Perpendicular states are plotted in inverted colors. $|H'\rangle$ and $|V'\rangle$ states were transmitted sufficiently. However $|D\rangle$ state had unwanted ellipticity at the output.

	S0	S1	S2	S3	$\psi[°]$	$\chi[°]$
$|H'\rangle$	1.0004 ± 0.0003	≈ -1	-0.016 ± 0.007	0.02 ± 0.01	-89.54	0.67
$|V'\rangle$	0.9912 ± 0.0002	0.99103 ± 0.00005	-0.004 ± 0.004	0.02 ± 0.01	-0.13	0.44
$|D'\rangle$	0.95 ± 0.01	-0.016 ± 0.008	-0.53 ± 0.01	-0.78 ± 0.01	-45.86	-27.88

Table 10: Output data table for welded cross-connection.

Connector key is usually aligned to slow axis. Second implementation requires special connector that has key aligned to fast axis. The second implementation is based on connecting these two connectors via mating sleeve. Required connector modification was done by Optokon. Advantage is that we do not need to do any welding. Disadvantage is need for fiber connector modification. Modified connectors are not standard and have to be made on demand.

We did the same analysis as before. The DOP was higher than 90%. Input and output states are plotted in Figure 17. Data are in Table 11. We see that $|H'\rangle$ and $|V'\rangle$ states were transmitted sufficiently as in previous implementation, but $|D'\rangle$, $|A'\rangle$, $|R'\rangle$ and $|L'\rangle$ states were changed - it seem this change makes difficult to distinguish between $|D'\rangle$ and $|L'\rangle$ and between $|A'\rangle$ and $|R'\rangle$. But this is not true because ellipticities of states $|D'\rangle$,$|L'\rangle$ and $|A'\rangle$, $|R'\rangle$ have
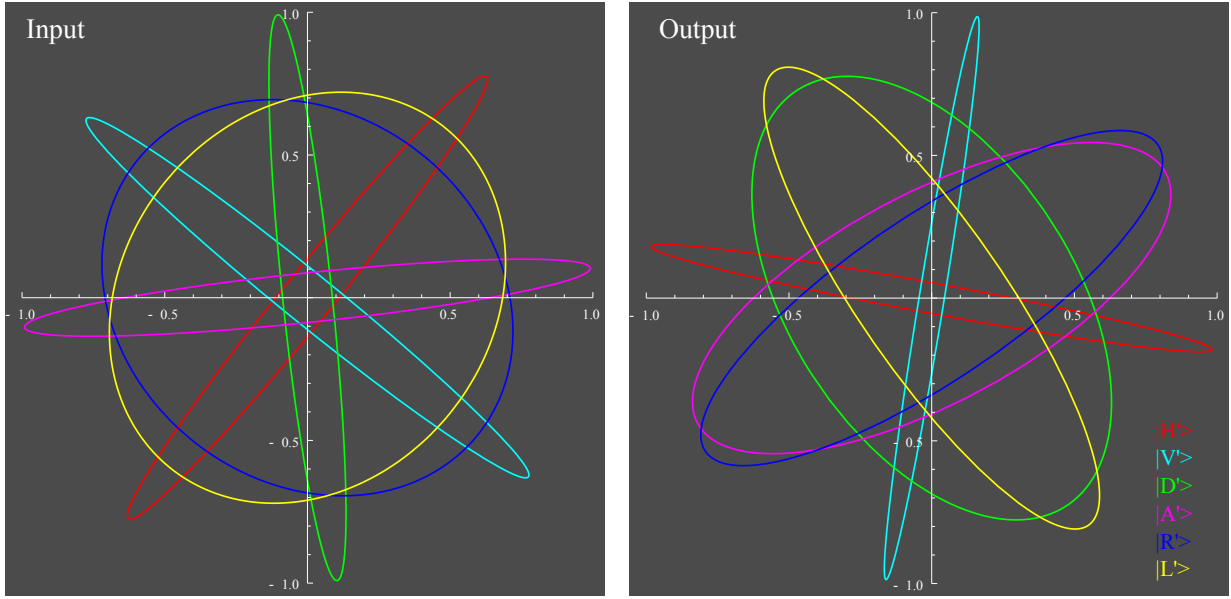
25

opposite sign.

Figure 17: Special connector implementation. We see that states were affected by ellipticity changes.

	S0	S1	S2	S3	$\psi[°]$	$\chi[°]$
$|H'\rangle$	0.9637 ± 0.0008	0.8956 ± 0.0005	-0.341 ± 0.002	0.103 ± 0.002	-10.42	3.06
$|V'\rangle$	0.9472 ± 0.0007	-0.8947 ± 0.0005	0.299 ± 0.002	-0.083 ± 0.002	80.75	-2.53
$|D'\rangle$	1.0 ± 0.1	-0.216 ± 0.007	-0.478 ± 0.006	0.9 ± 0.1	-57.15	29.86
$|A'\rangle$	0.98 ± 0.02	0.396 ± 0.007	0.60 ± 0.02	-0.67 ± 0.02	28.17	-21.49
$|R'\rangle$	0.908 ± 0.009	0.281 ± 0.009	0.705 ± 0.008	0.50 ± 0.01	34.11	16.68
$|L'\rangle$	0.99 ± 0.02	-0.304 ± 0.004	-0.80 ± 0.02	-0.49 ± 0.02	-55.39	-14.83

Table 11: Table contains output states data of the second implementation - the special connector.

Third implementation was using special FC/PC mating sleeve. The keyholes at the one end of the mating sleeve were rotated by 90 degrees to each other - see Figure 18. We will call this special mating sleeve a *cross-mating sleeve*.

Advantage is obvious: we can use standard PM fibers. Quality of transmission is naturally sensitive to precision of keyholes positioning. Sizes of connector keys may vary, keys may not fit into the cross-mating sleeve keyhole precisely causing axes misalignment - this is another disadvantage.
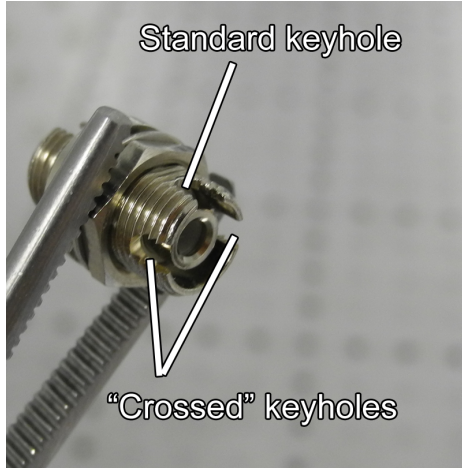
Figure 18: Special FC/PC mating sleeve. We used this coupler in third implementation of cross-connection. New keyholes are rotated approximately by 90 degrees with respect to standard keyholes.

We used PM fibers by OZ Optics because they had good results in the "series test" (see section 3.9). The worst DOP was however 86% for $|D'\rangle$ state. Other states propagated with DOP higher than 96%. See Figure 19 for polarization ellipses before and after propagation. Data are in Table 12. Compared with other cross-connection implementations we have similar results.

For entanglement distribution is important states orthogonality preservation. That is why we did following data analysis: Stokes vectors were transformed into Jones vectors and absolute value of inner product was calculated, the value represents orthogonality of polarized parts of states. This was done for pairs of formerly orthogonal states. See Table 13 for results.
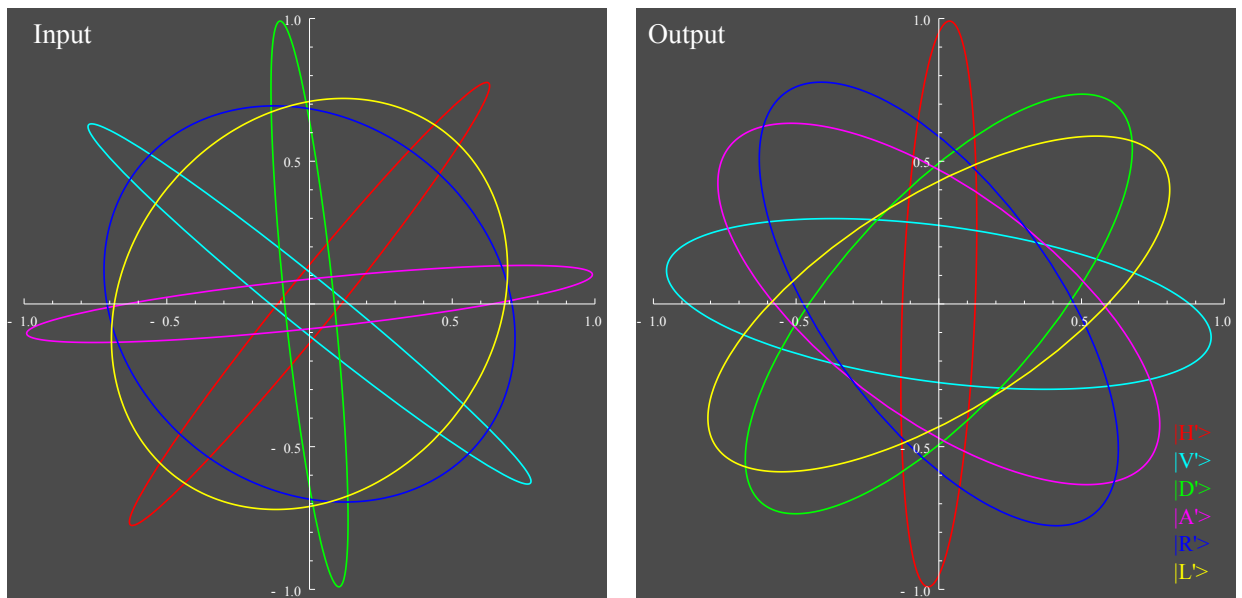

Figure 19: Cross-mating sleeve implementation. We see that states were affected by ellipticity changes. Ellipses of propagated $|D'\rangle$ and $|L'\rangle$ states are more similar than in second implementation.

	S0	S1	S2	S3	$\psi[°]$	$\chi[°]$
$|H'\rangle$	0.988 ± 0.003	-0.9528 ± 0.0009	0.07 ± 0.02	-0.25 ± 0.01	87.80	-7.32
$|V'\rangle$	1.00 ± 0.01	0.817 ± 0.002	-0.22 ± 0.01	0.52 ± 0.03	-7.58	15.86
$|D'\rangle$	0.86 ± 0.02	-0.07 ± 0.02	0.632 ± 0.009	0.57 ± 0.02	48.16	21.02
$|A'\rangle$	0.96 ± 0.02	0.19 ± 0.02	-0.63 ± 0.01	-0.70 ± 0.03	-36.60	-23.42
$|R'\rangle$	1.0 ± 0.1	-0.21 ± 0.01	-0.649 ± 0.009	0.7 ± 0.2	-53.98	23.84
$|L'\rangle$	1.01 ± 0.01	0.31 ± 0.02	0.65 ± 0.02	-0.703 ± 0.008	32.26	-22.09

Table 12: Output states for cross-mating sleeve implementation.

Implementation	$|\langle H'|V'\rangle|$	$|\langle D'|A'\rangle|$	$|\langle R'|L'\rangle|$
Welded cross-connection	0.0219	-	-
Special connector	0.0223	0.154	0.0332
Cross-mating sleeve	0.171	0.0774	0.0549

Table 13: We quantify orthogonality of polarized parts of two states as an absolute value of their inner product. Zero means perfect orthogonal states. Each implementation of cross-connection makes formerly orthogonal states a little less orthogonal.

Summary: By cross-connecting of PM fibers we can maintain high DOP at the output regardless the input polarization. According to Table 13 states remained orthogonal - this is good for entanglement transmission.
All tested implementations had similar results. Third implementation is the most convenient one - it is easy to use and it does not require special PM fibers. We would like to test more cross-mating sleeves in the future to see if we can get even better results.

4 Conclusion

In the first part of the thesis we tested properties of PM fibers. According to our measurements, we can achieve high degree of polarization, up to 99%, for well-aligned states. Achieved DOP depends on used coupling lens as we have investigated. We can however compensate lens influence by using quarter-wave plate.

Degree of polarization of a well-aligned state is also very stable and resistant to mechanical stress, highest tested deformation was 30mm bending diameter. These properties allows us to use polarization-maintaining fibers in further applications - polarization-sensitive components connections, fiber interferometers and so on.

A DOP-based polarization angular alignment method was introduced. It is convenient for broader-band spectra sources. Method allows achieving close-to-maximal DOP in order of minutes. Unlike other methods of polarization alignment, we do not need any polarimeter, oscilloscope or a heat source to perform DOP-alignment.

Last but not least we introduced and tested the cross-connection method which allows us maintain high DOP of arbitrary polarization state. Since the transmitted states remained orthogonal, we assume that PM fibers can be used to transmit polarization entanglement.

References

[1] SALEH, Bahaa E. A. - TEICH, Malvin Carl. *Fundamentals of photonics*. 2nd ed. Hoboken, N.J. : Wiley-Interscience, c2007. xix, 1177 s. Wiley series in pure and applied optics. ISBN 9780471358329.

[2] ČECHOVÁ, Marie. *Elektromagnetické vlny.* 2. vyd. Olomouc : Univerzita Palackého, 1993. 159 s. ISBN 80-7067-237-4.

[3] HUARD, Serge. *Polarization of light.* Chichester: John Wiley and Sons; Paris: Masson, 1997. xii, 333 s. ISBN 0471965367.

[4] DI DOMENICO, Gianni - WEIS, Antoine. *Light Polarization And StokesParameters*, Wolfram Demonstrations. Available from url (24/01/2013):
`http://demonstrations.wolfram.com/LightPolarizationAndStokesParameters/`

[5] ARORA, Poonam - AGARWAL, Ashish - GUPTA, Vinay. *Simple alignment technique for polarization-maintaining fibers.* Review Of Scientific Instruments 82, 125103 (2011).

[6] LIMPOUCH, Jan. *Úvod do počtu pravděpodobnosti*, ČVUT, 2000.

[7] *Product Data 905(P)/905(P)-E*, Evanescent Optics Inc. Available from url (04/05/2013):
`http://www.evanescentoptics.com/products.php?id=25`

A   Appendix

A.1   Modified Stokes parameters

Reader might be confused by relation (15). There is a conflict between "our" definition of DOP and definition of DOP from literature [3]. Either definitions of Stokes vector components (20) are not the same.

To prevent any more confusion we will use a prime symbol $'$ to mark definitions from [3]. Stokes vector components are defined by relations:

$$
\begin{aligned}
S_1' &= I_H - I_V, \\
S_2' &= I_D - I_R, \\
S_3' &= I_R - I_L, \\
S_0' &= I_H + I_V.
\end{aligned}
\tag{22}
$$

Degree of polarization is in literature defined as:

$$
DOP' = \frac{1}{S_0'}\sqrt{S_1'^2 + S_2'^2 + S_3'^2}.
\tag{23}
$$

At this point reader may notice that "our" Stokes vector components are dimensionless unlike those from literature that have dimension of optical intensity. With identity

$$
S_0' = I_H + I_V = I_D + I_A = I_R + I_L
$$

we can rewrite (20) using (22):

$$
\begin{aligned}
S_1 &= \frac{S_1'}{S_0'}, \\
S_2 &= \frac{S_2'}{S_0'}, \\
S_3 &= \frac{S_3'}{S_0'}.
\end{aligned}
\tag{24}
$$

Substituting (24) into (15) we can easily see that:

$$
DOP = \sqrt{S_1^2 + S_2^2 + S_3^2} = \sqrt{\left(\frac{S_1'}{S_0'}\right)^2 + \left(\frac{S_2'}{S_0'}\right)^2 + \left(\frac{S_3'}{S_0'}\right)^2} = \frac{1}{S_0'}\sqrt{S_1'^2 + S_2'^2 + S_3'^2} = DOP'.
$$

We just have proved that DOP defined in [3] is equivalent to relation (15) that we used.
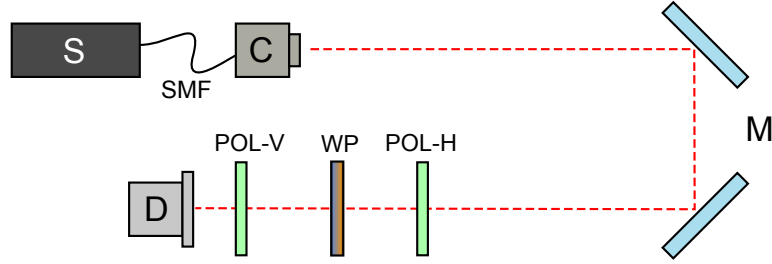
A.2   Wave plate mounts calibration

Figure 20: Callibration setup: S - laser source; SMF - single mode fiber; C - collimator; M - mirrors; POL-H - H-polarizer; WP - examined wave-plate in mount; POL-V - V-polarizer; D - detector.

Axes of the wave plate were unknown when mounting wave plate into mount, but we needed to have wave plate angle under control. That is why we had to do a mount calibration.

We crossed polarizers and put the tested wave plate in mount between them as shown in Figure 20. We scanned intensity as a function of mount angle. From the theory section we know that output intensity depends on angle of wave plate.

Equation (25) shows dependence of normalized intensity in case of HWP, equation (26) in case of QWP.

$$I_{HWP}(\alpha) = \langle H|(POL(90°)HWP(\alpha))^\dagger(POL(90°)HWP(\alpha))|H\rangle = \sin^2(2\alpha), \qquad (25)$$

$$I_{QWP}(\beta) = \langle H|(POL(90°)QWP(\beta))^\dagger(POL(90°)QWP(\beta))|H\rangle = \frac{1}{2}\sin^2(2\beta). \qquad (26)$$

When calibrating manual mounts, it is enough to rotate mounted wave plate until we reach minimal intensity on detector D. Then we note the mount angle which we consider as zero angle of wave plate.

We cannot apply this method on motorized mount because motorized mount do not have a scale, so we are not able to read angles and we do not want to rotate mount manually. Therefore we need to scan intensity as a function of mount angles. Then we fit function $f(x)$ to scanned data using parameters a, b, c. Function $f(x)$ has this form:

$$a\sin^2(2(x+c)) + b.$$

The parameter c is calibration parameter which we were looking for. Calibration data of HWP2 and function fit are shown in Figure 21. We calibrated the rest of motorized mounts the same way. Review of calibration parameters is in Table 14.
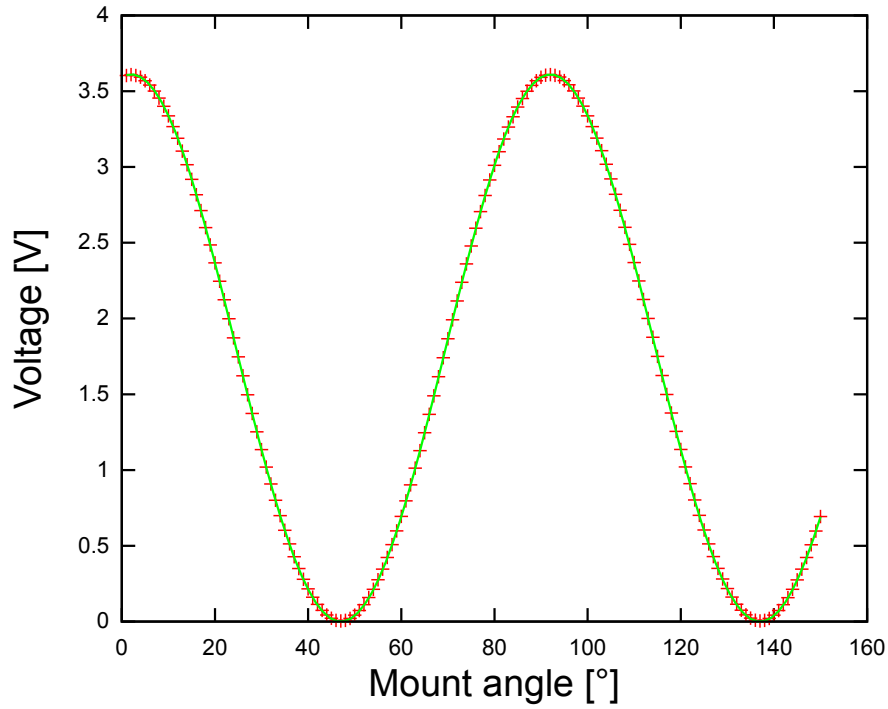
Figure 21: Data (red) of scanned HWP2 in motorized mount and fitted function (green). The parameter $c \approx 47.5\,^\circ$.

Version	c_{HWP1}	c_{QWP1}	c_{HWP2}	c_{QWP2}	Used in chapter(s):
4	32.5	89	47.5	23.5	3.10, 3.9
3	41	3	32.5	89	3.7
2	-	-	88.888	74.2771	3.8, 3.6, 3.5
1	-14.989	27.2753	88.888	74.2771	3.4

Table 14: Table of used calibration parameters according to version of setup. In the first version all wave plates were in motorized mounts (HWP1, QWP1 in Newport SR50CC; HWP2 and QWP2 in Newport PR50CC). In version two QWP1 and HWP1 were in manual mounts (Thorlabs RSP1). Third version used two precision manual mounts (Thorlabs PRM1) for HWP2 and QWP2 and two manual mounts (Thorlabs RSP1) for HWP1 and QWP1. The most recent version used precise manual mount (Thorlabs PRM1) for HWP1, QWP1 and motorized mounts (Newport SR50CC) for HWP2 and QWP2.

A.3   Used statistics

We were using standard statistic tools. Arithmetic mean was used to express mean value of data set $x = x_1, x_2, \ldots, x_n$:

$$\bar{x} = \frac{1}{n} \sum_{i=0}^{n} x_i. \tag{27}$$

We often used standard deviation which gave us variability characteristics of data set:

$$u(x) = \sigma = \sqrt{\frac{1}{(n-1)} \sum_{i=0}^{n} (\bar{x} - x_i)^2}. \tag{28}$$

When analysing data from non-direct measurement we used law of error propagation in form:

$$u(f(x, y, \ldots)) = \sqrt{\left(\frac{\partial f}{\partial x} u(x)\right)^2 + \left(\frac{\partial f}{\partial y} u(y)\right)^2 + \ldots}, \tag{29}$$

where $u(f)$ is uncertainty of function $f(x, y, \ldots)$, $x, y, \ldots$ are variables of function and $u_A(x)$, $u_A(y)$ are uncertainties of these variables.

Formula (29) applied on (20) gives us:

$$
\begin{aligned}
u(S_1) &= \frac{2}{I_V + I_H} \sqrt{I_V^2 u(I_H)^2 + I_H^2 u(I_V)^2}, \\
u(S_2) &= \frac{2}{I_A + I_D} \sqrt{I_A^2 u(I_D)^2 + I_D^2 u(I_A)^2}, \\
u(S_3) &= \frac{2}{I_R + I_L} \sqrt{I_L^2 u(I_R)^2 + I_R^2 u(I_D)^2}.
\end{aligned}
\tag{30}
$$

We are able to proof that:

$$u(S_0) = \frac{1}{S_0} \sqrt{S_1^2 u(S_1^2) + S_2^2 u(S_2^2) + } \tag{31}$$

Formulas (30) and (31) were used on estimating mean values and deviations of Stokes vector components. Data set was obtained by repeated measurement of tomography projection intensity (at each projection were recorded 10 intensities). Obtained uncertainty does not not take in count deviations in wave plates setting, long term laser or noise fluctuations or any other non-trivial sources of errors.

A.4   Tables

Implementation: Welded fibers

	HWP1 $\alpha[°]$	QWP1 $\beta[°]$	$\psi[°]$	$\chi[°]$
$|H'\rangle$	58	-	51	0
$|V'\rangle$	13	-	-39	0
$|D'\rangle$	35.5	-	6	0

Implementation: Rotated key

	HWP1 $\alpha[°]$	QWP1 $\beta[°]$	$\psi[°]$	$\chi[°]$
$|H'\rangle$	55	50	51	-5
$|V'\rangle$	100.5	50	-39	5
$|D'\rangle$	78	95	-84	-5
$|A'\rangle$	33	5	6	-5
$|R'\rangle$	33	50	-39	-40
$|L'\rangle$	78	50	51	40

Implementation: Cross-mating sleeve

	HWP1 $\alpha[°]$	QWP1 $\beta[°]$	$\psi[°]$	$\chi[°]$
$|H'\rangle$	323.5	42.75	43.75	-1.75
$|V'\rangle$	8.5	42.75	-46.25	1.75
$|D'\rangle$	346	87.75	88.75	-1.75
$|A'\rangle$	301	-2.25	-1.25	-1.75
$|R'\rangle$	301	42.75	-46.25	-43.25
$|L'\rangle$	346	42.75	43.75	43.25

Table 15: Characteristics of input states corresponding to tables 10, 11 and 12. HWP1 and QWP1 are physical mount angles of preparation apparatus, ψ is position of polarization ellipse and χ is its ellipticity. Angle values are in degrees.

OZ Optics

ID	HWP+QWP DOP[%]	HWP-only DOP [%]	Note
t16078212	100.0 ± 0.3	87.7 ± 0.4	Connector B
t16078212	99.8 ± 0.2		Connector A
t16078215	99.9 ± 0.2	85.64 ± 0.08	Connector A
t16078215	99.9 ± 0.2		Connector B
t16078214	99.7 ± 0.1	87.45 ± 0.08	A
t16078214	99.6 ± 0.1		B
t16078112	99.7 ± 0.2	85.31 ± 0.05	A
t16078112	99.69 ± 0.02		B
t16078111	99.09 ± 0.02	85.71 ± 0.09	B
t16078111	99.79 ± 0.01		A
t16078113	99.75 ± 0.04		A
t16078113	99.5 ± 0.2	88.9 ± 0.1	B
t16078312	99.8 ± 0.5	87.5 ± 0.4	A
t16078312	99.83 ± 0.05	87.5 ± 0.3	B
t16078313	99.72 ± 0.05	88.7 ± 0.2	A
t16078313	99.8 ± 0.1	85.8 ± 0.1	B
t16078311	99.7 ± 0.2	87.8 ± 0.1	A
t16078311	99.7 ± 0.1	87.30 ± 0.07	B
t16078412	99.77 ± 0.02	87.13 ± 0.05	A
t16078412	99.49 ± 0.03	84.97 ± 0.04	B
Mean	99.7	87	Data set
Deviation	0.2	1	statistics

SQS

ID	HWP+QWP DOP[%]	HWP-only DOP [%]	Note
0100728720	99.71 ± 0.01	86.72 ± 0.04	connectors
0100728719	99.74 ± 0.03	89.18 ± 0.04	reffers to
0100728718	99.78 ± 0.02	86.8 ± 0.2	ID
0100728722	99.53 ± 0.01	87.38 ± 0.08	
0100728877	99.93 ± 0.04	87.70 ± 0.08	
0100727884	99.90 ± 0.01	86.84 ± 0.07	
Mean	99.7	87.4	Data set
Deviation	0.1	0.9	statistics

Table 16: Maximal achieved DOP with and without QWP1 at the input. Various PM fibers were tested. DOP-based alignment method was used. Mean and deviation value are referring to dataset of measured PM fibers, unlike deviations of single PM fiber which is calculated from intensity fluctuations using standard error-propagation.
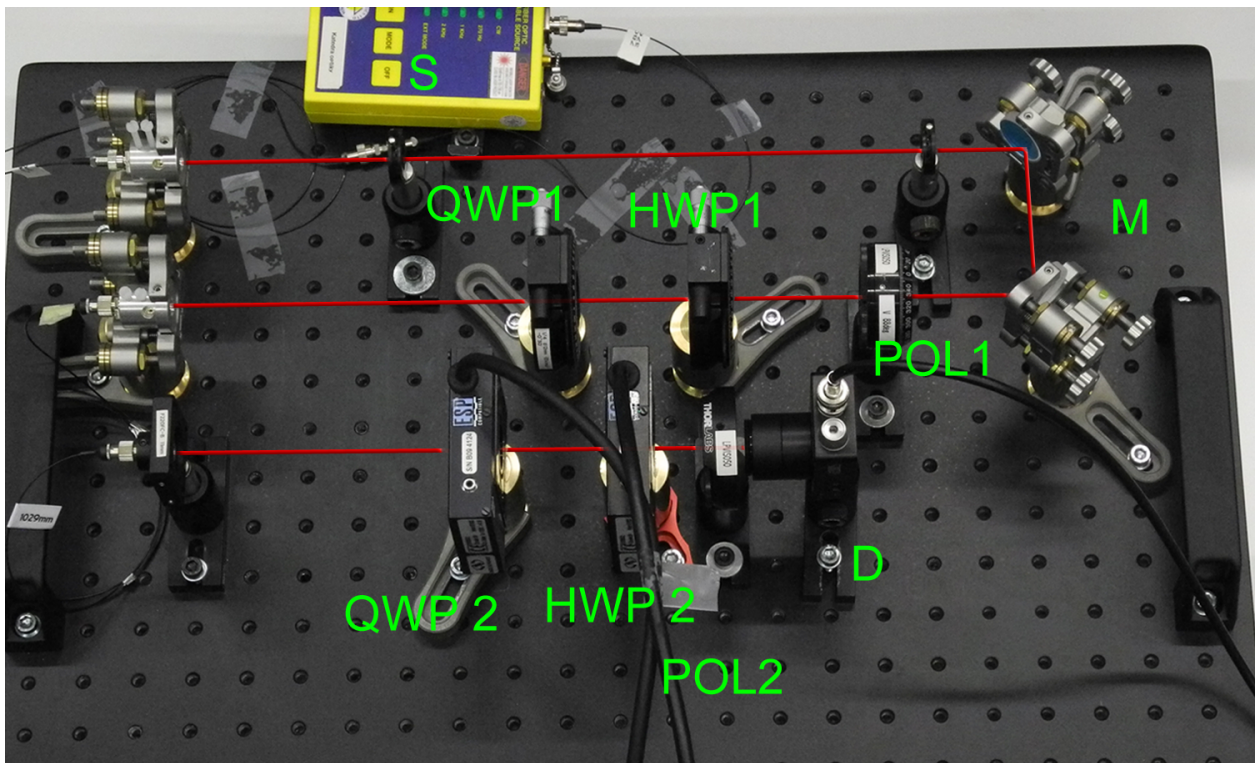
A.5 Figures

Figure 22: Implementation of core-setup. Green labels are corresponding to the scheme in Figure 5, red line illustrates beam. S - laser diode; M - mirrors; POL1 - polarizer; HWP1 - half-wave plate, QWP1 - quarted-wave plate, QWP2 - quarter-wave plate; HWP2 - half-wave plate, POL2 polarizer; D - PIN diode.
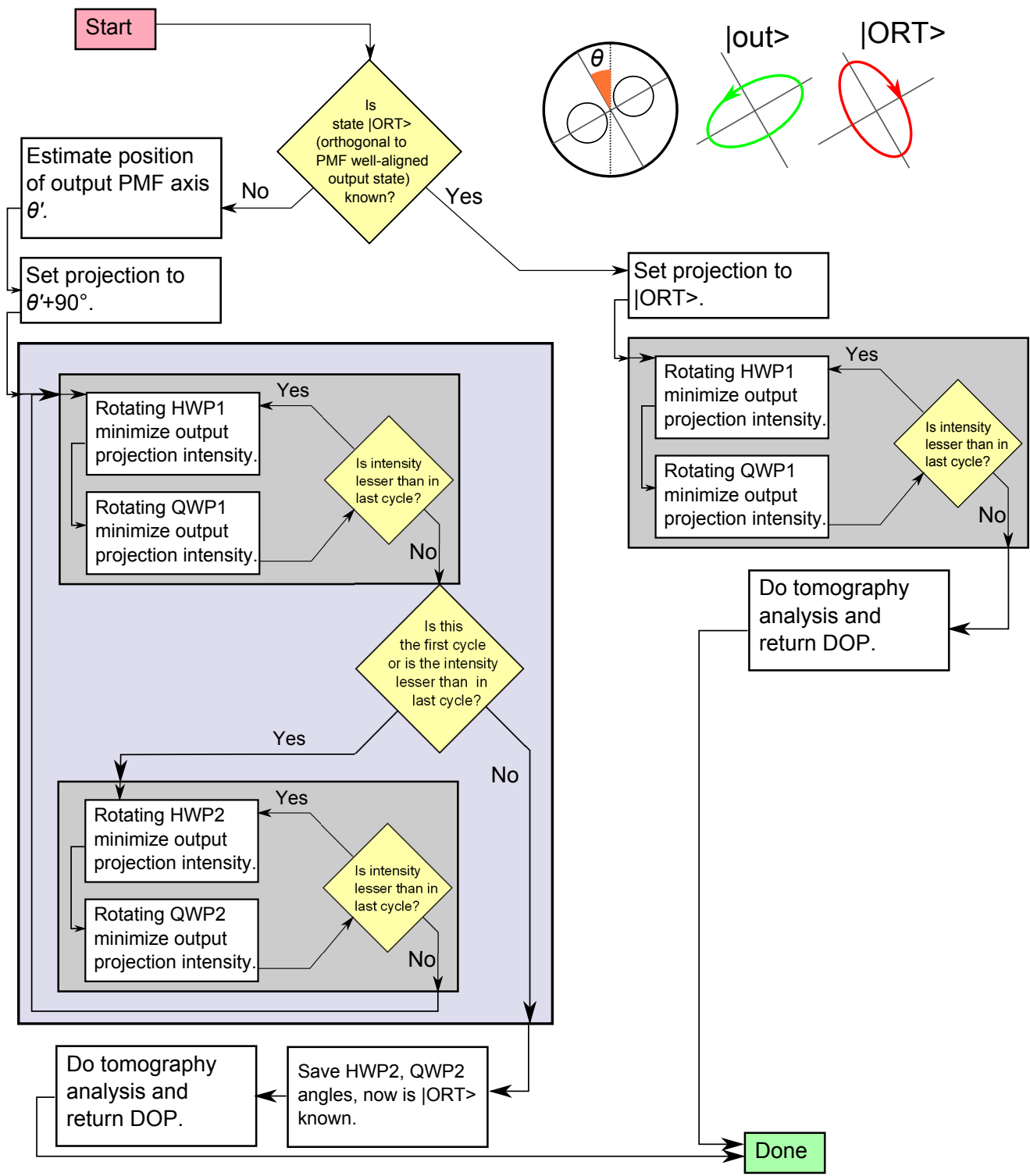
Figure 23: Second version alignment method. This version takes in count elliptical state at the output of PM fiber. It is slower than first version. DOP improvement in comparison with first version is dependent on ellipticity caused by decoupling lens.

A.6   List of used parts

- Laser diode source, OZ optics FOSS-01-3S-5/125-810-S-1
  `http://www.ozoptics.com/ALLNEW_PDF/DTS0019.pdf`

- Single mode optical fiber, Thorlabs 780HP
  `http://thorlabs.com/thorcat/6800/6829-S01.pdf`

- Polarization-maintaining optical fiber (PM fiber)
  Oz optics, SQS, Optokon
  Various pieces were tested

- Collimator, Schäfter + Kirchhoff, 60F-011-02, 11 mm lens
  Various pieces were tested.

- Collimator, Thorlabs F220FC-B, 10.99 mm lens
  `http://www.thorlabs.de/thorproduct.cfm?partnumber=F220FC-B`

- Polarizers
  Thorlabs LPVIS050
  `http://thorlabs.com/NewGroupPage9.cfm?ObjectGroup_ID=752`

- Half-wave plate (HWP), Eksma 810nm, 812nm

- Qarter-wave plate (QWP), Eksma 810nm
  Waveplate were mounted in Newport motorized mounts, or Thorlabs manual mounts were used.

- PIN diode (D), Thorlabs DET36A/m
  `http://thorlabs.com/thorProduct.cfm?partNumber=DET36A/M`

- Multimeter, Aim&TTi 1906
  `http://www.tti-test.com/products-tti/pdf-brochure/prec-1906-4p.pdf`

- Detector kit (D)
  Coherent FieldMaster-GS with LM2-VIS diode sensor
  `http://www.coherent.com/downloads/FieldMasterGSUserManual.pdf`
  `http://www.coherent.com/products/?704/High-Sensitivity-Optical-Sensors-RoHS`

- Manual high-precision waveplate mount
  Thorlabs PRM1
  `http://www.thorlabs.de/thorProduct.cfm?partNumber=PRM1`

- Manual waveplate mount
  Thorlabs RSP1
  `http://www.thorlabs.de/thorProduct.cfm?partNumber=RSP1`

- Motorized waveplate mount - fast
  Newport PR50PP
  `http://search.newport.com/?q=*&x2=sku&q2=PR50PP`

- Motorized waveplate mount
  Newport SC50CC
  `http://search.newport.com/?q=*&x2=sku&q2=SR50CC`

- Motorized mounts controller
  Newport SMC100
  `http://www.newport.com/SMC100-Single-Axis-Motor-Controller-Driver/400968/1033/info.aspx`